International Journal of Physical Sciences

Volume 8 Number 29 9 August, 2013
ISSN 1992-1950

Academic Journals

ABOUT IJPS

The **International Journal of Physical Sciences (IJPS)** is published weekly (one volume per year) by Academic Journals.

International Journal of Physical Sciences (IJPS) is an open access journal that publishes high-quality solicited and unsolicited articles, in English, in all Physics and chemistry including artificial intelligence, neural processing, nuclear and particle physics, geophysics, physics in medicine and biology, plasma physics, semiconductor science and technology, wireless and optical communications, materials science, energy and fuels, environmental science and technology, combinatorial chemistry, natural products, molecular therapeutics, geochemistry, cement and concrete research, metallurgy, crystallography and computer-aided materials design. All articles published in IJPS are peer-reviewed.

Submission of Manuscript

Submit manuscripts as e-mail attachment to the Editorial Office at: ijps@academicjournals.org. A manuscript number will be mailed to the corresponding author shortly after submission.

For all other correspondence that cannot be sent by e-mail, please contact the editorial office (at ijps@academicjournals.org).

The International Journal of Physical Sciences will only accept manuscripts submitted as e-mail attachments.

Please read the **Instructions for Authors** before submitting your manuscript. The manuscript files should be given the last name of the first author.

Editorial Board

Instructions for Author

Electronic submission of manuscripts is strongly encouraged, provided that the text, tables, and figures are included in a single Microsoft Word file (preferably in Arial font).

The **cover letter** should include the corresponding author's full address and telephone/fax numbers and should be in an e-mail message sent to the Editor, with the file, whose name should begin with the first author's surname, as an attachment.

Article Types

Three types of manuscripts may be submitted:

Regular articles: These should describe new and carefully confirmed findings, and experimental procedures should be given in sufficient detail for others to verify the work. The length of a full paper should be the minimum required to describe and interpret the work clearly.

Short Communications: A Short Communication is suitable for recording the results of complete small investigations or giving details of new models or hypotheses, innovative methods, techniques or apparatus. The style of main sections need not conform to that of full-length papers. Short communications are 2 to 4 printed pages (about 6 to 12 manuscript pages) in length.

Reviews: Submissions of reviews and perspectives covering topics of current interest are welcome and encouraged. Reviews should be concise and no longer than 4-6 printed pages (about 12 to 18 manuscript pages). Reviews are also peer-reviewed.

Review Process

All manuscripts are reviewed by an editor and members of the Editorial Board or qualified outside reviewers. Authors cannot nominate reviewers. Only reviewers randomly selected from our database with specialization in the subject area will be contacted to evaluate the manuscripts. The process will be blind review.

Decisions will be made as rapidly as possible, and the journal strives to return reviewers' comments to authors as fast as possible. The editorial board will re-review manuscripts that are accepted pending revision. It is the goal of the IJPS to publish manuscripts within weeks after submission.

Regular articles

All portions of the manuscript must be typed double-spaced and all pages numbered starting from the title page.

The Title should be a brief phrase describing the contents of the paper. The Title Page should include the authors' full names and affiliations, the name of the corresponding author along with phone, fax and E-mail information. Present addresses of authors should appear as a footnote.

The Abstract should be informative and completely self-explanatory, briefly present the topic, state the scope of the experiments, indicate significant data, and point out major findings and conclusions. The Abstract should be 100 to 200 words in length.. Complete sentences, active verbs, and the third person should be used, and the abstract should be written in the past tense. Standard nomenclature should be used and abbreviations should be avoided. No literature should be cited.

Following the abstract, about 3 to 10 key words that will provide indexing references should be listed.

A list of non-standard **Abbreviations** should be added. In general, non-standard abbreviations should be used only when the full term is very long and used often. Each abbreviation should be spelled out and introduced in parentheses the first time it is used in the text. Only recommended SI units should be used. Authors should use the solidus presentation (mg/ml). Standard abbreviations (such as ATP and DNA) need not be defined.

The Introduction should provide a clear statement of the problem, the relevant literature on the subject, and the proposed approach or solution. It should be understandable to colleagues from a broad range of scientific disciplines.

Materials and methods should be complete enough to allow experiments to be reproduced. However, only truly new procedures should be described in detail; previously published procedures should be cited, and important modifications of published procedures should be mentioned briefly. Capitalize trade names and include the manufacturer's name and address. Subheadings should be used. Methods in general use need not be described in detail.

Results should be presented with clarity and precision. The results should be written in the past tense when describing findings in the authors' experiments. Previously published findings should be written in the present tense. Results should be explained, but largely without referring to the literature. Discussion, speculation and detailed interpretation of data should not be included in the Results but should be put into the Discussion section.

The Discussion should interpret the findings in view of the results obtained in this and in past studies on this topic. State the conclusions in a few sentences at the end of the paper. The Results and Discussion sections can include subheadings, and when appropriate, both sections can be combined.

The Acknowledgments of people, grants, funds, etc should be brief.

Tables should be kept to a minimum and be designed to be as simple as possible. Tables are to be typed double-spaced throughout, including headings and footnotes. Each table should be on a separate page, numbered consecutively in Arabic numerals and supplied with a heading and a legend. Tables should be self-explanatory without reference to the text. The details of the methods used in the experiments should preferably be described in the legend instead of in the text. The same data should not be presented in both table and graph form or repeated in the text.

Figure legends should be typed in numerical order on a separate sheet. Graphics should be prepared using applications capable of generating high resolution GIF, TIFF, JPEG or Powerpoint before pasting in the Microsoft Word manuscript file. Tables should be prepared in Microsoft Word. Use Arabic numerals to designate figures and upper case letters for their parts (Figure 1). Begin each legend with a title and include sufficient description so that the figure is understandable without reading the text of the manuscript. Information given in legends should not be repeated in the text.

References: In the text, a reference identified by means of an author‘s name should be followed by the date of the reference in parentheses. When there are more than two authors, only the first author‘s name should be mentioned, followed by ’et al‘. In the event that an author cited has had two or more works published during the same year, the reference, both in the text and in the reference list, should be identified by a lower case letter like ’a‘ and ’b‘ after the date to distinguish the works.

Examples:

Abayomi (2000), Agindotan et al. (2003), (Kelebeni, 1983), (Usman and Smith, 1992), (Chege, 1998; 1987a,b; Tijani, 1993,1995), (Kumasi et al., 2001)

References should be listed at the end of the paper in alphabetical order. Articles in preparation or articles submitted for publication, unpublished observations, personal communications, etc. should not be included in the reference list but should only be mentioned in the article text (e.g., A. Kingori, University of Nairobi, Kenya, personal communication). Journal names are abbreviated according to Chemical Abstracts. Authors are fully responsible for the accuracy of the references.

Examples:

Ogunseitan OA (1998). Protein method for investigating mercuric reductase gene expression in aquatic environments. Appl. Environ. Microbiol. 64:695-702.

Gueye M, Ndoye I, Dianda M, Danso SKA, Dreyfus B (1997). Active N2 fixation in several Faidherbia albida provenances. Ar. Soil Res. Rehabil. 11:63-70.

Charnley AK (1992). Mechanisms of fungal pathogenesis in insects with particular reference to locusts. In: Lomer CJ, Prior C (eds) Biological Controls of Locusts and Grasshoppers: Proceedings of an international workshop held at Cotonou, Benin. Oxford: CAB International, pp 181-190.

Mundree SG, Farrant JM (2000). Some physiological and molecular insights into the mechanisms of desiccation tolerance in the resurrection plant Xerophyta viscasa Baker. In Cherry et al. (eds) Plant tolerance to abiotic stresses in Agriculture: Role of Genetic Engineering, Kluwer Academic Publishers, Netherlands, pp 201-222.

Short Communications

Short Communications are limited to a maximum of two figures and one table. They should present a complete study that is more limited in scope than is found in full-length papers. The items of manuscript preparation listed above apply to Short Communications with the following differences: (1) Abstracts are limited to 100 words; (2) instead of a separate Materials and Methods section, experimental procedures may be incorporated into Figure Legends and Table footnotes; (3) Results and Discussion should be combined into a single section.

Proofs and Reprints: Electronic proofs will be sent (e-mail attachment) to the corresponding author as a PDF file. Page proofs are considered to be the final version of the manuscript. With the exception of typographical or minor clerical errors, no changes will be made in the manuscript at the proof stage.

International Journal of Physical Sciences

Table of Contents: Volume 8 Number 29 9 August, 2013

ARTICLES

CHEMISTRY

MATERIAL SCIENCES

academicJournals

Vol. 8(29), pp. 1494-1505, 9 August, 2013
DOI: 10.5897/IJPS2013.3966
ISSN 1992 - 1950 © 2013 Academic Journals
http://www.academicjournals.org/IJPS

International Journal of Physical Sciences

Full Length Research Paper

Theoretical study on structural and electronic properties of 4-[(E)-[4-(trifloromethyl)-1,3-benzothiazol-2-yl]azo]naphthalen-1-ol and 1-[(E)-[4-(trifloromethyl)-1,3-benzothiazol-2-yl]azo]naphthalen-2-ol using density functional theory (DFT)

Bello Isah Adewale and Semire Banjo*

Department of Pure and Applied Chemistry, Ladoke Akintola University of Technology, P. M. B. 4000, Ogbomoso, Oyo state, Nigeria.

Accepted 19 July, 2013

In this work, the structural and electronic properties of 4-[(E)-[4-(trifloromethyl)-1,3-benzothiazol-2-yl]azo]naphthalen-1-ol (*ortho*-OH) and 1-[(E)-[4-(trifloromethyl)-1,3-benzothiazol-2-yl]azo]naphthalen-2-ol (*para*-OH) using density functional theory (DFT) were presented. The calculated vibrational frequencies were compared very well with experimental. The total energy for the isomers A and B were -4277242.55 and -4277216.21 kJ/mol respectively; thus structural relaxation was observed in isomer A which resulted into extra thermodynamic stability over isomer B by 26.34 kJ/mol. ^{13}C and ^{1}H NMR chemical shifts for two isomers were calculated and compared. Electrophilicity index revealed that isomer A would be mote reactive towards nucleophiles more than isomer B.

Key words: 4-[(E)-[4-(trifloromethyl)-1,3-benzothiazol-2-yl]azo]naphthalen-1-ol, 1-[(E)-[4-(trifloromethyl)-1,3-benzothiazol-2-yl]azo]naphthalen-2-ol, electronic properties, density functional theory (DFT).

INTRODUCTION

Among the classes of dyes, azo-dyes are of particular interest to chemists because they can be easily prepared with a wide range of donor and acceptor substituents; in addition, the planarity of the azo bridge is expected to enhance electronic delocalization, and consequently the optical activity (Almeida et al., 2010). Azo dyes have found extensive applicability in analytical chemistry as acid-base, redox and metallochromic indicators (Zollinger, 1987; Perez et al., 2000; Geogiadou and Tsatsaroni, 2001). The nature of aromatic substituents on both sides of the azo group is another important parameter that controls the colours of the azo compounds, water-solubility and binding ability on a particular fabric (Pavia et al., 1998). All of azo dyes contain at least one azo (-N=N-) group, which links two sp^2 –hybridized carbon atoms in the molecular structures. Also, the cis and trans isomers of azo compounds have served as a model for the photochromic compounds (Grebenkin and Bolshakov, 1999; Yang et al., 2001; Tamai and Miasaka, 2000; Azuki et al., 2001).

The prediction of molecular and spectroscopic properties of dye molecules is an important part in the designing process. Computational chemistry methods offer a unique ability for organic chemists to generate optimal geometry of structures and to calculate spectroscopic properties that are of higher accuracy. One

*Corresponding author. E-mail: bsemire@lautech.edu.ng.

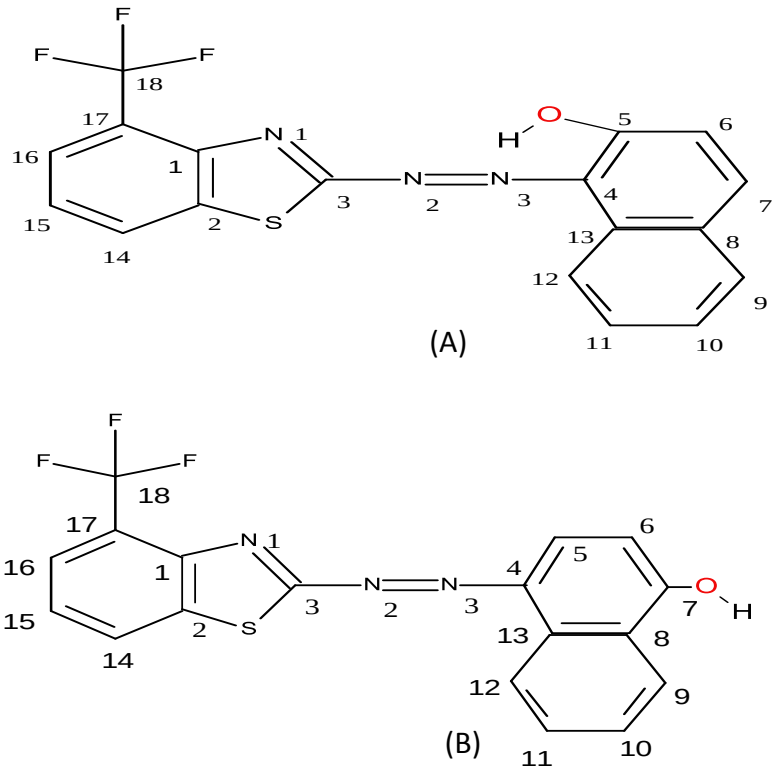

Figure 1. The schematic structure and numbering of the studied compounds: (A) = 1-[(E)-[4-(triflоromethyl)-1,3-benzothiazol-2-yl]azo]naphthalen-2-ol (*ortho*-OH) and (B) = 4-[(E)-[4-(triflоromethyl)-1,3-benzothiazol-2-yl]azo]naphthalen-1-ol (*para*-OH).

of the most widely used computational chemistry methods is density functional theory (DFT). In this work, attempt is made to study the effect of hydroxyl group (-OH) at *ortho* and *para* positions on the geometry, the vibrational frequencies, reactivity and maximum absorption peaks (λ_{max}) of the studied dye isomers using DFT (Figure 1).

COMPUTATIONAL METHODS

The molecular structures of the 1-[(E)-[4-(triflоromethyl)-1,3-benzothiazol-2-yl]azo]naphthalen-2-ol (*ortho*-OH) and 4-[(E)-[4-(triflоromethyl)-1,3-benzothiazol-2-yl]azo]naphthalen-1-ol (*para*-OH) in the ground state were optimized by Becke 3-Lee-Yang-Parr (B3LYP) level with 6-31G* basis set (Becke, 1993; Perdew et al., 1996) on an Intel(R) Core (TM) i3-2350M/2.30 GHz with 4.0 GB RAM personal computer using Spartan 06. The absorption transitions were calculated from the optimized geometry in the ground state S_0 using configuration interaction (CI) theory. The harmonic vibrational frequency calculations resulting in IR frequency together with intensities and chemical shifts of the considered compounds were calculated at the same level. It has been shown that B3LYP applications are successful in shielding calculations on carbon atoms (Bello et al., 2009). Dipole moments and atomic partial charges originated from Mulliken population analysis are also reported.

RESULTS AND DISCUSSION

Geometries and stability

The selected geometrical parameters were listed in Table 1. The S1-C2 (S1-C3) bond length calculated was 1.738 (1.779Å) for *ortho*-OH and 1.749 (1.789Å) for *para*-OH respectively; this showed that S1-C2 and S1-C3 are shortened in *ortho*-OH by 0.011 and 0.010Å respectively. The N2=N3 and N3-C4 were 1.278 and 1.369Å for *ortho*-OH and 1.273 and 1.390Å for *para-OH* respectively, that is, N3-C4 was lengthened by 0.021Å and N2=N3 was shortened by 0.005 in *ortho*-OH respectively. Hydrogen bonding between –OH group and N3 of azo group with bond length of 1.962Å was observed in *ortho*-OH isomer. The bond angles calculated for the two *ortho*-OH and *para*-OH isomers were quite similar in values except bond angles around azo group. For instance, C3-N2-N3 and N2-N3-C4 were 112.52 and 121.53° for *ortho*-OH whereas in *para*-OH isomers they were 113.38 and 122.89° respectively. These differences in bond angles around azo group bring about planarity differences in the molecules as reflected in their dihedral angles (Table 1).

The calculations revealed that *ortho-OH* isomer was

Table 1. The selected geometries (bond length (Å), bond angle (º), dihedral angle (º) of the studied dyes at B3LYP/6-31G*.

Bond length	A	B
S_1-C_3	1.779	1.789
S_1-C_2	1.738	1.749
N_1=C_3	1.301	1.300
C_3-N_2	1.391	1.392
N_2=N_3	1.278	1.273
N_3-C_4	1.369	1.390
N3…HO	1.962	-
Bond angle		
C_2-S_1-C_3	88.17	88.16
N_1-C_3-S_1	116.20	116.21
S_1-C_3-N_2	114.52	114.00
N_1-C_3-N_2	129.28	129.79
C_3-N_2-N_3	112.52	113.38
N_2-N_3-C_4	121.35	122.89
Dihedral angle		
C_1-N_1-C_3-S_1	0.00	-0.32
C_2-S_1-C_3-N_1	-0.00	0.38
S_1-C_3-N_2-N_3	-180.00	176.48
N_1-C_3-N_2-N_3	0.00	-3.58
C_3-N_2-N_3-C_4	180.00	-179.99
N_2-N_3-C_4-C_5	180.00	178.81
N_2-N_3-C_4-C_{13}	0.00	-0.88
N3-H-O-C5	179.75	-

more planar than *para-OH* isomer which was not in agreement with what had been reported (Bello et al., 2009). The planarity of dye A (*ortho*-OH) could be explained in terms of hydrogen bond that was formed between OH group hydrogen and N3 of azo group which resulted into partial rotational restriction of naphthenyl rings.

This argument was further supported by 179.75° dihedral angle calculated for N3-H-O-C5. Therefore, the OH group on isomer A (*ortho*-OH) was along the plane of naphthenyl rings while that of isomer B (para-OH) rotates at approximately -178° as shown in Figure 2. This rotation of naphthenyl rings in isomer B has little effect on the planarity of 4-trichloromethyl-1,3-benzothiazolyl substructure of the molecule (Table 1). The largest deviation in dihedral angles for isomers A and B was 3.58° in N1-C3-N2-N3. The total energy for the isomers A and B were -4277242.55 and -4277216.21 kJ/mol respectively; this implied that structural relaxation observed in isomer A resulted into extra thermodynamic stability over isomer B with about 26.34 kJ/mol (Table 2). The solvation energy and PSA were -36.14 kJ/mol and 38.85Å^2 for isomer A and -43.84 kJ/mol and 40.86Å^2 for isomer B respectively.

Electronic properties

The HOMO, LUMO, band gap, dipole moment, total energy, salvation energy and polar surface area (PSA) for the *ortho*-OH and *para*-OH isomers were listed in Table 2. The HOMO and LUMO are important parameters that provide reasonable qualitative information about the excitation properties of molecules. The HOMO and LUMO calculated for isomer A were -5.88 and -2.97 eV, while that for isomer B were -5.72 and -2.82 eV respectively. Therefore, OH group at *para* position in isomer B resulted to stabilization of both HOMO and LUMO by ≈ 0.15 eV as compared to isomer A. The molecular energy levels for both isomers were displayed in Figure 2 which comprised of eight HOMOs and two LUMOs for each molecule. The HOMO and LUMO are very important parameters for molecular reactivity. The HOMO is the orbital with electrons thereby acts as electron donor and the LUMO is the unoccupied orbital thus acts as the electron acceptor. The gap between HOMO and LUMO characterizes the molecular chemical stability. The HOMO-1 and HOMO-2 differed in energy by 0.1 eV, while HOMO-4 and HOMO-5, HOMO-6 and HOMO-7 differed in energy by 0.2 eV for isomer A

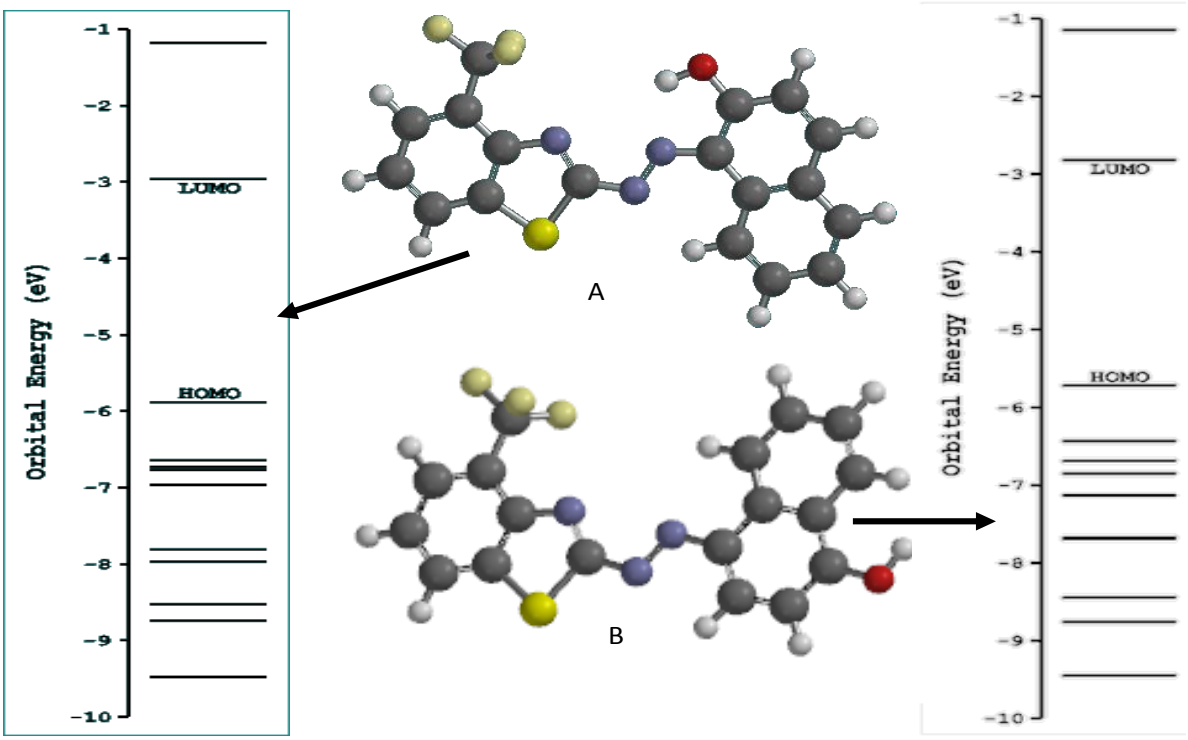

Figure 2. Optimized structures and molecular orbital energy levels of the *ortho*-OH and *para*-OH using the basis set B3LYP/6-31G*.

Table 2. Standard thermodynamic (at 298 K and 1atm) and electronic properties of the studied compounds.

Parameter	A (*ortho*-OH)	B (*para*-OH)
HOMO (eV)	-5.88	-5.72
LUMO (eV)	-2.97	-2.82
Band gap (eV)	2.91	2.90
Dipole moment (debye)	3.70	2.78
$\eta = \left[\frac{H-L}{2}\right]$	1.455	1.45
$\mu = -\left[\frac{H+L}{2}\right]$	-4.425	-4.27
Softness (1/ 2η)	0.3436	0.3448
$\omega = \left[\frac{\mu^2}{2\eta}\right]$	6.7287	6.287
ENERGY(kJ/mol)	-4277242.55	-4277216.21
Rel. Energy	0.00	26.34
Solvation energy (kJ/mol)	-36.14	-43.84
PSA (Å^2)	38.85	40.86
ZPE (kJ/mol)	655.00	652.11
H^o (kJ/mol)	701.96	700.15
S^o (J/mol)	540.05	548.19
G^o (kJ/mol)	540.94	536.70
Ovality	1.49	1.50
logP	1.94	6.62
polarizability	67.03	67.06

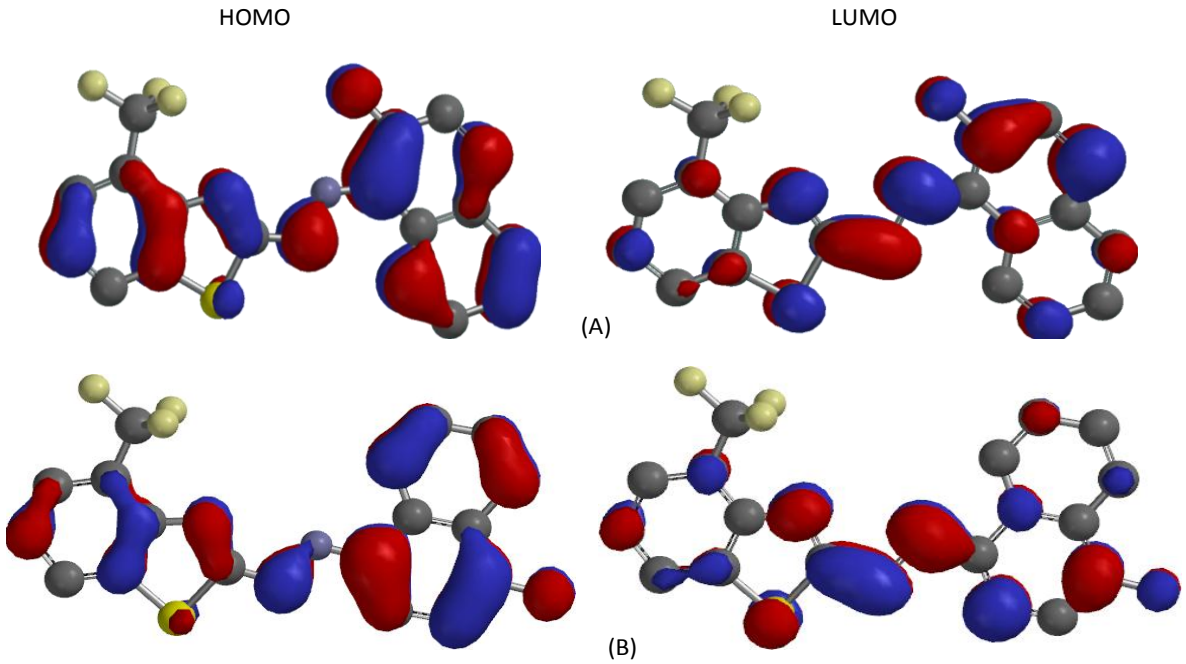

Figure 3. The HOMO and the LUMO diagram: A = *ortho*-OH and B = *para*-OH.

(ortho-OH). However, only HOMO-2 and HOMO-3 were close in isomer B (para-OH) with energy difference of 0.2 eV. Figure 3 showed that both HOMO and LUMO map of the two isomers spread over the entire molecule. The HOMO was C=C bonding and C-C anti-bonding while the LUMOs were C-C bonding and C=C anti-bonding for the isomers.

The electronic properties of the molecules are calculated from the total energies and the Koopmans' theorem. The ionization potential is (IP) determined from the energy difference between the energy of the compound derived from electron transfer which is approximated; IP =E_{HOMO} while the electron affinity (EA) is given as; EA =E_{LUMO}, respectively. The other important quantities such as chemical potential (μ), chemical hardness (η) and electrophilicity index (ω) are deduced form IP and EA values (Zhou and Navangul, 1990; Chamizo et al., 1993; Bird, 1997; Koopmans, 1934; Parr et al., 1999; Pearson, 1993). The values of chemical potential, chemical hardness, softness, and electrophilicity index for isomer A were 4.425, -1.455, 0.3436 and 6.7287 eV respectively and that of isomer B were 4.270, -1.450, 0.3448 and 6.287 eV respectively, therefore would be better propensity of isomer A to be involved in the interactions with nucleophiles than for isomer B. The dipole moment in a molecule is another important electronic property. For example, the bigger the dipole moment, the stronger the intermolecular interactions expected. The calculated dipole moment values for the isomers were 3.70 and 2.78 D for Isomers A and B respectively.

Table 3. The selected Mulliken charges of compounds.

Parameter	*ortho*-OH (A)	*para*–OH (B)
N_1	-0.483	-0.463
N_2	-0.335	-0.298
N_3	-0.377	-0.310
C_2	0.266	0.263
C_3	-0.125	-0.125
S	0.241	0.239
C_8	0.304	0.297
C_4	0.227	0.231
O	-0.619	-0.624

The Mulliken charges of the two isomers were displayed in Table 3 and Figure 4. The Mulliken charges on nitrogen atoms revealed that azo nitrogen atoms were negative in values, thus they are center for electrophilic attack/ attachment during dyeing. The Mullikan changes on azo nitrogen atoms (N2=N3) of isomer A were higher than that of isomer B. These higher charges observed were also reflected on C3 and sulphur atoms of isomers A which might be due to the presence of hydrogen bond as earlier discussed. The Mulliken charges on hydroxyl oxygen of isomer A also supported this postulate. The charges on hydroxyl oxygen of isomer A was reduced by 0.005 as compared to that of isomer B, which means some of the charges on oxygen atoms of isomer A have been transferred through hydrogen bond to azo group (Table 3).

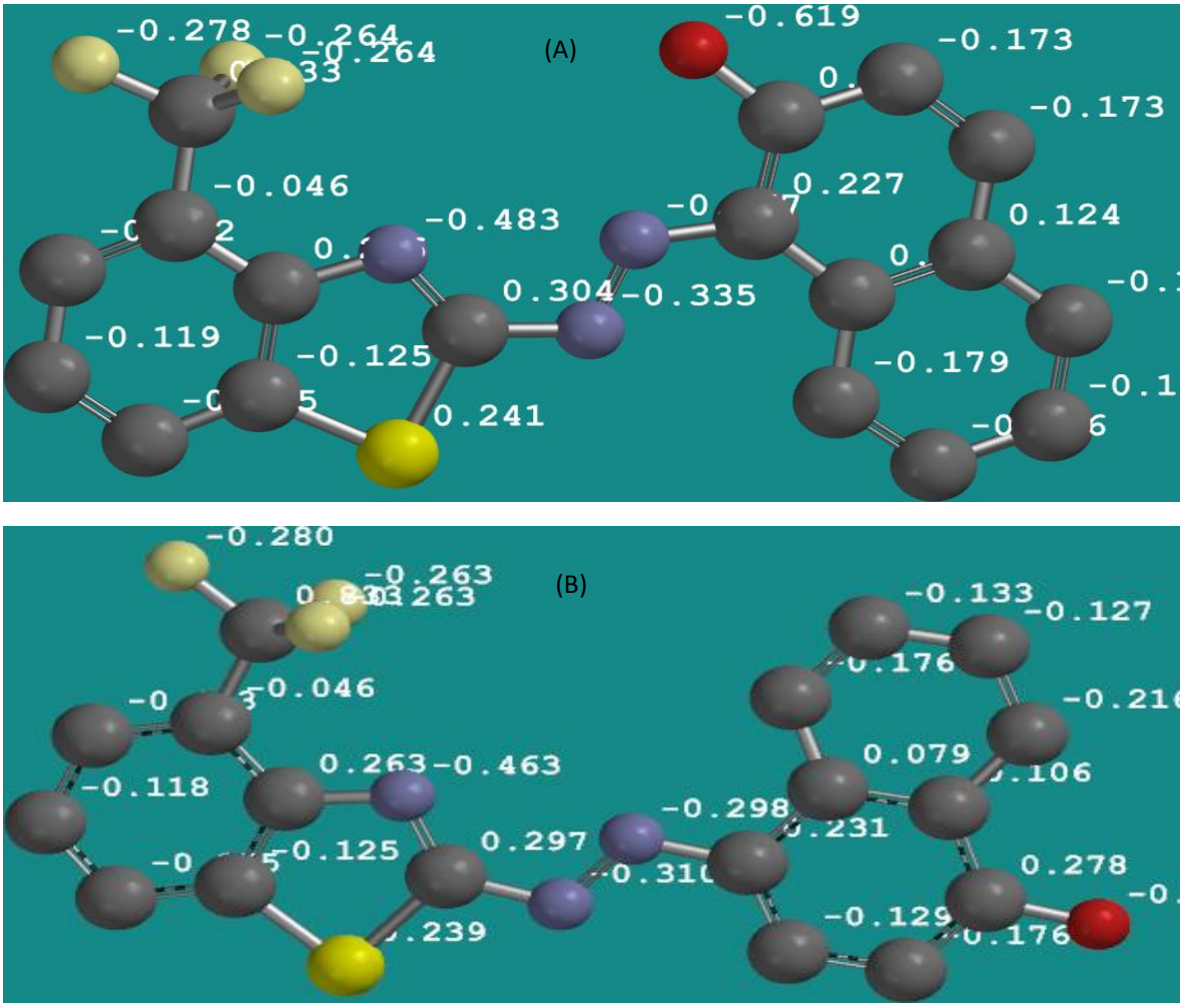

Figure 4. Calculated Mulliken charges as displaced on the compounds; (A) = *ortho*-OH isomer and (B) = *para*-OH isomer.

Table 4. The experimental and theoretical absorption wavelength for *ortho*-isomer (A) and *para*-isomer (B).

Isomer	Acetone (λ_{max}) nm	Ethanol (λ_{max}) nm	Ethanol + HCl (λ_{max}) nm	Δ(λ_{max}) ethanol-(HCl/ethanol)	(λ_{max}) nm DFT/6-31G*/CIS
Ortho (A)	482	486	492	+6	288.70, 416.32, 496.82
Para (B)	484	489	492	+3	338.21, 416.69, 522.04

The experimental and calculated adsorption λ_{max} (nm) for the *ortho*-OH and *para*-OH isomers were shown in Table 4. The calculated adsorption spectra showed three λ_{max} which was the characteristics of aromatic multiple rings in a molecule. The third absorption λ_{max} agreed with the experimentally observed values (Bello et al., 2009). The calculated absorption λ_{max} were 288.70, 416.32 and 496.82 nm for *ortho*-OH isomer as compared to *para*-OH isomer with 338.21, 416.69 and 522.04 nm. The experimental observed values for *ortho*-OH isomer were 482, 486 and 492 nm in acetone, ethanol and ethanol+HCl respectively. For *para*-OH isomer, the values were 484, 489 and 492 nm in acetone, ethanol and ethanol+HCl respectively. The theoretical order of adsorption λ_{max} prediction were in agreement with that observed experimentally, but more closer in values to λ_{max} that was observed the ethanol (Table 5). The differences in the calculated and experimental values were 15, 11 and 4 nm for isomer A; and 38, 33 and 30 nm for isomer B in acetone, ethanol and ethanol+HCl

Table 5. Experimental and Theoretical vibrational frequencies (cm^{-1}) computed at B3LYP/6-31G* level.

Ortho-isomer (A)		Para-isomer (B)		
DFT	**Expt.**	**DFT**	**Expt.**	**Assignment**
3429 (48.29)	3443	3767 (110.77)	3375	υOH
3273 (5.89)		3241 (3.54)		υ(CH)Ph
3236 (7.20)	3055	3240 (6.80)	3059	υ(CH)Ph
3231 (5.63)	3051	3237 (2.60)	3050	υ(CH)Ph
3217 (18.25)		3218 (13.10)		υ(CH)Ph
3211 (36.35)		3128 (16.29)		υ(CH)Ph
3202 (0.68)		3212 (25.64)		υ(CH)Ph
3195 (21.14)		3202 (1.27)		υ(CH)Ph
3192 (2.39)		3197 (12.90)		υ(CH)Ph
3183 (2.68)		3156 (25.10)		υ(CH)Ph
1668 (58.47)		1679 (15.23)		υ(C=C)Ph
1649 (93.94)	1624	1649 (7.47)	1624	υ(C=C)Ph
1647 (1.98)	1610	1642 (139.53)	1601	υ(C=C)Ph
1624 (81.11)		1624 (109.76)		υ(C=C)Ph
1620 (30.08)		1620 (40.22)		υ(C=C)Ph
1581 (59.37)		1572 (136.09)		υ(C=C)Ph
1540 (106.76)	1512	1541 (65.52)	1512	υN=N + υC=N
1522 (25.19)		1521 (5.80)		υ(C=C)Ph
1518 (39.33)		1504 (143.12)		υ(C=C)Ph
1496 (11.22)	1462	1493 (19.08)	1460	υ(C=C)Ph + δCH(Ph)
1472 (324.23)		1472 (200.95)		υN=N + δCH(Ph)
1452 (38.20)		1442 (140.50)		υC=C + δCH(Ph) + δOH
1436 (110.27)		1434 (3.55)		υC=N + δCH(Ph) + δOH
1425 (157.28)		1417 (44.46)		υN=N + υC=N + δCH(Ph)
1389 (8.86)		1399 (294.33)		υC=C
1384 (36.47)		1364 (78.22)		υC=C
1344 (196.21)		1340 (168.30)		υC-N + υC-C
1335 (271.84)	1332	1332 (41.92)	1320	υC=C + υC-N + υC-C + δCH(Ph)
1329 (148.85)	1320	1320 (46.83)	1318	υC-O + υC-C + δCH(Ph)
1317 (28.60)		1305 (46.87)		υC-N + υ(C=C)Ph + υ(CH)Ph
1272 (189.35)		1278 (356.75)		υC-N + δOH + υ(CH)Ph
1252 (59.10)	1242	1240 (149.63)	1238	υC-S + δCH(Ph) + υCF
1241 (170.64)		1220 (220.35)		υC=C + υCF
1231 (43.90)	1218	1207 (160.83)	1210	C-S + δCH(Ph) + δOH
1206 (116.75)		1206 (123.75)		υCF + δCH(Ph)
1201 (248.91)		1202 (238.17)		υCF
1194 (29.19)		1196 (30.31)		δCH(Ph)
1184 (83.09)		1186 (25.80)		υCF + δCH(Ph)
1174 (1.10)		1183 (153.79)		δCH(Ph)
1151 (330.01)		1156 (395.76)		υC-N + δCH(Ph)
1114 (52.27)		1100 (59.13)		υC-N + δCH(Ph)
1099 (41.59)		1093 (31.68)		υC-S + υCF
1088 (82.03)		1083 (20.86)		δ_{ring}
1035 (10.46)		1067 (60.86)		δCH(Ph)
1009 (0.53)		1043 (7.70)		δ_{ring}
985 (0.78)		1019 (0.58)		πCH
975 (2.11)	972	991 (0.37)	985	πCH
961 (0.96)		979 (2.54)		πCH
944 (31.26)	869	970 (42.52)	873	υC-S
923 (1.38)		951 (0.30)		πCH

Table 5. Contd

898 (0.45)		928 (1.42)		
888 (1.95)		872 (1.76)		πCH
849 (18.23)	851	871 (1.20)	858	πCH + πOH
829 (12.57)		862 (25.58)		
808 (113.13)	792	847 (37.56)	796	πOH
797 (26.29)		804 (3.07)		πCH
787 (12.74)	752	800 (29.45)	780	πCH
771 (15.29)	735	787 (0.01)	740	πCH
760 (16.12)		763 (18.35)		πCH + πC-N
747 (10.31)		762 (48.17)		δ_{ring}
713 (11.29)		757 (11.04)		δ_{ring}
711 (22.73)		725 (29.70)		$\delta CF + \delta_{ring}$
698 (5.58)		713 (15.61)		πCH + πC-N
685 (33.78)		687 (24.79)		
643 (0.45)	624	666 (0.34)	628	πN=C-N
623 (2.09)		644 (4.92)		τ_{ring}
619 93.90)		634 (11.56)		πCH(Ph)
612 (2.20)		630 (3.89)		πCH(ph)
596 (16.00)	553	601 (1.40)	557	τOH

υ, stretching; δ, in-plane bending; π, out of plane bending; ρ, rocking; τ, twisting.

respectively. The differences might be due to the level of theoretical method used and also that calculations were performed in isolated state or gas phase, while the properties were measured in liquid state.

Vibrational frequencies

Vibrational spectroscopy is one of the powerful methods extensively used in organic chemistry for the identification of functional groups of organic compounds and also used to distinguish molecular conformers, tautiomers and isomers (Silverstein et al., 1981). The use of theoretical vibrational modes coupled with the theoretical results help to understand a fairly complex system, therefore some of the observed experimental vibrational frequencies and the theoretically calculated vibrational frequencies were shown in Table 5 for comparison. The calculated vibrational frequencies were found to be in good agreement with the experimentally observed ones, although the calculated frequencies were slightly higher than the observed values for the majority of the normal modes. The factors responsible for these discrepancies are due to: first environmental conditions and the second one arise from the fact that the experimental value is an anharmonic frequency while the calculated value is a harmonic frequency. The theoretical results can be improved as compared to the experimental by scaling the theoretical results (Devlin et al., 1995; Teimouri et al., 2008; Palafox et al., 2007; Tarcan et al., 2009).

The experimentally observed aromatic C–H stretching vibrations for the two isomers were 3055 and 3051 cm^{-1} for ortho-isomer A, and 3059 and 3050 cm^{-1} for para-isomer B which are still within 2900 to 3064 cm^{-1} region assigned for aromatic C–H stretching vibrations (Varsanyi, 1969; Kayitha et al., 2010; Usha et al., 2010; Rastogi et al., 2010). These vibrations were calculated to be in the 3273-3183 cm^{-1} region for ortho-OH isomer and 3241-3156 cm^{-1} region for para-OH isomer. The C–H in-plane bending vibrations were theoretically observed at 1114 to1335 cm^{-1} region in isomer A and 1100 to 1332 cm^{-1} for isomer B; however these vibrational bands were not pure as observed theoretically. The C–H out-of-plane bending vibrations were calculated to be in the region 898 to 612 and 1019 to 630 cm^{-1} for isomers A and B; these were experimentally observed in the 972 to 851 cm^{-1} for isomer A and 985-858 cm^{-1} for isomer B.

The stretching vibrations of OH group of the isomers were observed experimentally 3444 and 3375 cm^{-1} for isomer A and B respectively. These were calculated to be 3429 and 3767 cm^{-1} isomer A and B respectively. The OH stretching vibrations intensity for isomers A and B were 48.29 and 110.77; therefore isomer B has higher intensity by about 120% which was in agreement with observed hydrogen bond in isomer A. The vibrations of OH in-plane (δOH) were in-pure as calculated in the gas phase, however, they were predominantly 1272 and 1231 cm^{-1} for isomer A, and 1278 and1207 cm^{-1} for isomer B. The out of plane (πOH) deformations calculated were in good agreement with experimental values. For instance, πOH calculated for isomers A and B were 808 and 847 cm^{-1} with 113.13 and 37.51 intensity respectively. These

Table 6. Computed ^{1}H and ^{13}C chemical shift in ppm at B3LYP/6-31G* level of calculations.

Isomer A (*ortho*-OH)				Isomer B (*para*-OH)			
Atom	**Ch. shift**	**Atom**	**Ch. shift**	**Atom**	**Ch. shift**	**Atom**	**Ch. Shift**
C1	150.94	*H5	4.26	C1	150.22	H5	8.18
C2	138.74	H6	6.53	C2	141.77	H6	6.94
C3	181.20	H7	7.76	C3	178.36	*H7	5.59
C4	141.08	H9	8.30	C4	143.56	H9	7.26
*C5	154.46	H10	7.34	C5	114.24	H10	7.57
C6	110.82	H11	7.22	C6	111.54	H11	7.73
C7	133.17	H12	7.40	*C7	160.74	H12	7.47
C8	121.13	H14	7.84	C8	121.28	H14	7.84
C9	117.66	H15	7.32	C9	117.23	H15	7.28
C10	125.65	H16	7.50	C10	125.57	H16	7.56
C11	130.03	N1	-53.59	C11	128.54	N1	-96.36
C12	124,32	N2	108.63	C12	127.69	N2	83.25
C13	131.31	N3	156.63	C13	136.89	N3	172.40
C14	125,12	S	347.74	C14	124.56	S	306.90
C15	126.17			C15	123.74	O	211.00
C16	124.20			C16	124.97		
C17	129.15			C17	129.39		
C18	124.16			C18	124.25		

*carbon bearing OH group or hydroxyl hydrogen.

were experimentally observed at 792 and 796 cm^{-1} for isomers A and B respectively. The torsion vibrations (τOH) were recorded at 553 and 557 cm^{-1} for the isomers A and B; however these were calculated to be 596 and 601 cm^{-1} in isomers A and B respectively.

The azo N=N stretching vibrations of the two isomers were recorded at 1535 and 1538 for isomers A and B respectively. These bands were calculated to be 1540 and 1472 for isomer A with 106.76 and 324.23 in intensity respectively. For isomer B, they were calculated at 1541 and 1472 cm^{-} with 65.52 and 200.95 in intensity respectively. The C-N and C=N stretching of the two isomers were calculated to be in 1436 to 1114 cm^{-1} region for isomer A and 1434 to 1100 cm^{-1} region for isomer B. The pure C-S stretching vibrations were calculated to be 869 and 873 cm^{-1} for isomers A and B respectively. However, these vibrations were observed theoretically coupled with other vibrations such as δCH(ph), δ(OH) and υ(CF). The pure υ(CF) vibrations was calculated to be 1201 cm^{-1} with 248.91 intensity for isomer A and 1202 cm^{-1} with 238.17 intensity for isomer B. The ring deformation (δ_{ring}) were calculated to be 1088, 1009, 747 and 713 cm^{-1} for isomer A, and 1083, 1043, 762 and 757 cm^{-1} for isomer B. The ring torsion (τ_{ring}) was calculated to be 623 cm^{-1} for isomer A and 644 cm^{-1} for isomer B.

^{1}HNMR and ^{13}CNMR in ppm

The molecular structure of the optimized isomers of the studied dyes at B3LYP method with 6-31G* basis set was used to calculate chemical shift for the dyes as shown in Table 6. It has been reported that ^{13}C and ^{1}H NMR calculated using DFT are in good agreement with the experimental (Cheeseman et al., 1996; Teimouri et al., 2008; Karakurt et al., 2012). Therefore, in the absence of experimental ^{13}C and ^{1}H NMR data for the two isomers, calculated NMR for the two isomers were comparatively discussed. The chemical shift for N1, N2, N3, S, and O atoms were -53.59, 108.63, 156.63, 347.74 and 213.88 ppm respectively for isomer A, while that of isomer B were -96.36, 83.25, 172.40, 306.90 and 206.00 ppm for N1, N2, N3, S, and O atoms respectively. The result in Table 6 showed that the ^{13}C NMR chemical shift of the two dye isomers are greater than 100 ppm which is the typical ^{13}C NMR chemical shift for organic molecule (Pihlaja and Kleinpeter, 1994; Kalinowski et al., 1988). The chemical shift of C3 and C4 `were 181.20 and 141.08 ppm for isomer A, and 178.36 and 143.56 for isomer B, therefore C3 experienced more de-shielding effect than all other carbon atoms because of its position in the molecule. It has been reported that presence of electronegative atom attracts all electron clouds of carbon atoms towards the electronegative atom, which in turn leads to de-shielding of carbon atom and result in increase in chemical shift values (Varsanyi and Sohar, 1972). This de-shielding effect was noticed in C5 and C7 for isomers A and B respectively because of the attachment of hydroxyl oxygen atom in each molecule respectively.

Table 7. The thermodynamic properties obtained at different temperature for the two isomers at B3LYP/6-31G* level.

	Isomer A			Isomer B		
Temp (K)	$C_{p,m}^o$ (cal/mol)	H_m^o (Kcal/mol)	S_m^o (cal/mol)	$C_{p,m}^o$ (cal/mol)	H_m^o (Kcal/mol)	S_m^o (cal/mol)
273	72.8298	166.08	124.03	74.28	165.64	126.16
373	96.1568	173.45	143.57	97.29	173.05	148.18
473	115.5856	182.55	162.18	116.46	182.14	163.76
573	130.9656	192.99	179.02	131.63	192.58	180.42
673	143.0138	204.32	194.27	143.53	203.84	193.54
773	152.5501	216.21	207.76	152.94	215.68	208.68
873	160.2175	228.53	219.53	160.51	227.95	220.28
973	166.4795	241.01	229.89	166.69	240.35	230.37

The signals of the aromatic proton are observed at 5 to 7 ppm (Pihlaja and Kleinpeter, 1994; Kalinowski et al., 1988) and it has been found that presence of electrons on aromatic ring, double bonded atoms, and triple bonded atoms has been found to de-shield attached hydrogen (Varsanyi and Sohar, 1972). Hydrogen atom is the smallest of all atoms and mostly localized on periphery of molecules, therefore their chemical shifts would be more susceptible to intermolecular interactions as compared to that for other heavier atoms. The hydroxyl groups of the two isomers are bounded to aromatic ring, one at *ortho*-position (isomer A) and the other at *para*-position (isomer B). The hydroxyl oxygen atom showed electronegative property hereby contributes to hydrogen atom downfield resonance which was more pronounced at *ortho* position as reflected in the computed ^{1}H chemical shift at 4.26 ppm for isomer A and 5.59 ppm for isomer B respectively. This might be the effect of hydrogen bonding in isomer A.

Thermodynamics properties

The thermodynamic properties calculated at 298.15 K in the ground state for the two isomers were shown in Table 2. The zero point energy (ZPE) for isomers A and B were 655.0 and 652.11 kJ/mol respectively. The standard enthalpy (H°), standard entropy (S°) and standard free energy (G°) were 701.96, 540.05 and 540.94 kJ/mol for isomer A (othro-OH) and 700.15, 548.19 and 536.70 kJ/mol for isomer B (para-OH). On the basis of vibrational analysis, the statically thermodynamic functions such as heat capacity ($C_{p,m}$°), entropy (S_m°) and enthalpy (H_m°) for the two isomers were obtained from the theoretical harmonic frequencies as listed in Table 7. All the $C_{p,m}^o$, S_m^o and H_m^o increased with the increase in temperature from 273 to 973 K; this was due to the enhancement of molecular vibrations while temperature increases at constant pressure (1 atm). The correlations between these thermodynamic parameters and temperature (T) were plotted (Figures 5, 6 and 7) and fitted by quadratic equations. The fitting factor (R^2) for these parameters for isomer A was found to be 0.999, 0.999 and 1 for heat capacity, enthalpy and entropy respectively. For isomer B, the fitting factor (R^2) was found to be 0.999 for all the thermodynamic parameters as shown in equations below:

Isomer A

$C_{p,m}^o = -0.268 + 0.310T - 0.000T^2 \times 10^{-4}$; (R^2= 0.999)

$H_m^o = 146.7 + 0.057T + 4.00T^2 \times 10^{-5}$ (R^2 = 0.999)

$S_m^o = 61.01 + 0.252T - 8.00 \times 10^{-5}T^2$ (R^2 = 1)

Isomer B

$C_{p,m}^o = 2.167 + 0.306T - 0.000T^2 \times 10^{-4}$; (R^2= 0.999)

$H_m^o = 146.1 + 0.058T + 4.00T^2 \times 10^{-5}$ (R^2 = 0.999)

$S_m^o = 67.55 + 0.238T - 7.00 \times 10^{-5}T^2$ (R^2 = 0.999)

All the thermodynamic calculations were performed in the gas phase; therefore recommended scale factors (Zhang et al., 2010) were used for better accurate prediction. All these thermodynamic data would be helpful in providing information for further study of the two isomers which could be useful to determine the directions of chemical reactions according to the second law of thermodynamics (Yazıcıet al., 2011; Govindarajana et al., 2012; Nataraj et al., 2013).

Conclusion

The structure of the 4-[(E)-[4-(trifloromethyl)-1,3-benzothiazol-2-yl]azo]naphthalen-1-ol and 1-[(E)-[4-(trifloromethyl)-1,3-benzothiazol-2-yl]azo]naphthalen-2-ol dyes were optimized by B3LYP/6-31G* level of theory and vibrational frequencies were calculated at the same level of theory. The global minimum energy between the two isomers showed that isomer A was thermodynamically more stable. It was found that the calculated vibrational frequencies were in good agreement with that of the experimental data. The UV-absorption wavelengths calculated by B3LYP/6-31G*/CIS agreed well with the experimental values, the slight differences were due the level of theoretical method used and also that calculations were performed in gas phase.

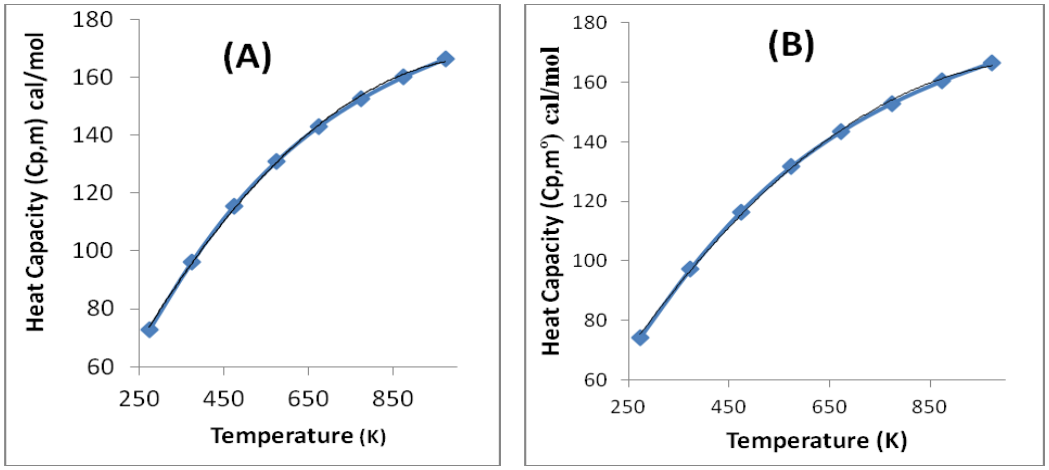

Figure 5. Correlation graph of heat capacity and temperature; (A) = ortho-OH and (B) = para-OH.

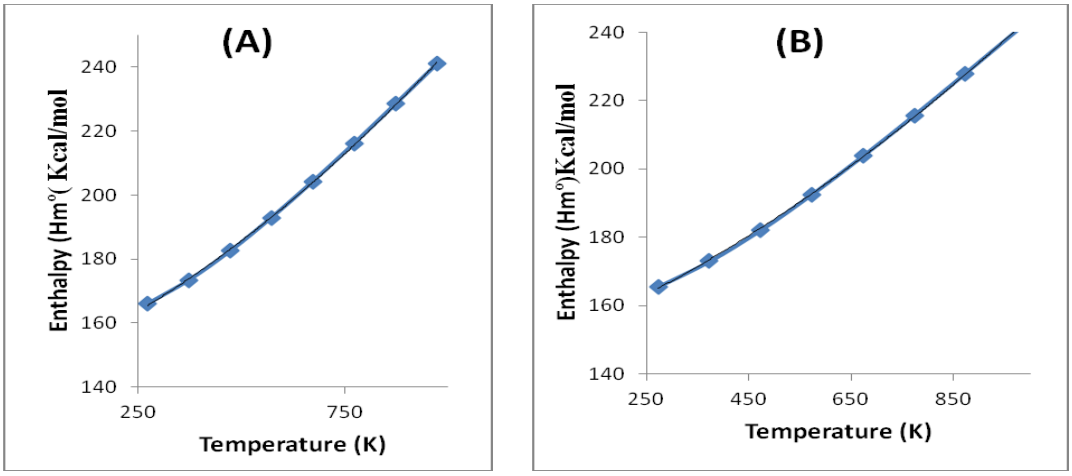

Figure 6. Correlation graph of enthalpy and temperature; (A) = ortho-OH and (B) = para-OH.

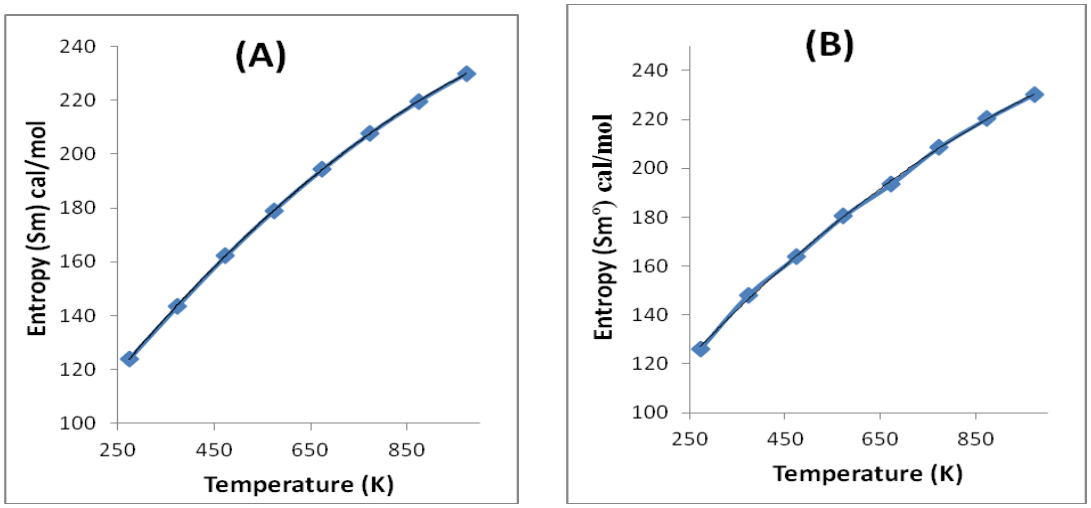

Figure 7. Correlation graph of entropy and temperature; (A) = ortho-OH and (B) = para-OH.

The correlations between the statistical thermodynamics and temperature revealed that the heat capacities, entropies and enthalpies increased with the increasing temperature due to the intensities of the molecular vibrations which increase with increasing temperature.

REFERENCES

Almeida MR, Stephani R, Dos Santos HF, de Oliveira LF (2010). Spectroscopic and theoretical study of the "azo"-dye E124 in condensate phase: evidence of a dominant hydrazo form. J. Phys. Chem. A. 114:526-534.

Azuki M, Morihashi K, Watanabe T, Taskahashi O, Kikuchi O (2001). Ab initio study of the acid-catalyzed cis-trans isomerization of methyl yellow and methyl orange in aqueous solution. J. Mol. Struct. Theochem. 542:255-262.

Becke AD (1993). Density-functional thermochemistry. III. The role of exact exchange J. Chem. Phys. 98:1372-1377.

Bello IA, Bello KA, Peters OA, Bello OS (2009). Synthesis, Spectroscopic, Thermodynamic And Dyeing Properties Of Disperse Dyes Derived From 2-Amino-4-Trifluoromethylbenzothiazole. Report and Opinion 1:58-66.

Bird CW (1997). Heteroaromaticity. 10. The Direct Calculation of Resonance Energies of Azines and Azoles from Molecular Dimensions. Tetrahedron. 53:13111-13118.

Chamizo JA, Morgado J, Sosa O (1993). Organometallic Aromaticity, Organometalliks., 12:5005-5007.

Cheeseman JR, Trucks GW, Keith TA, Frisch MJ (1996). A Comparison of Models for Calculating Nuclear Magnetic Resonance Shielding Tensors, J. Chem. Phys. 104:5497-5509.

Devlin FJ, Finley JW, Stephens PJ, Frisch MJ (1995). *Ab Initio* Calculation of Vibrational Absorption and Circular Dichroism Spectra Using Density Functional Force Fields: A Comparison of Local, Non Local, and Hybrid Density Functionals, J. Phys. Chem. 99:16883-16902.

Geogiadou KL, Tsatsaroni EG (2001). synthesis, characterization and application of disperse dyes derived from N-2-hydroxyethyl-1-naphthylamine", Dyes and Pigments, 50:93-100.

Govindarajana M, Karabacak M, Periandy S, Tanuja D (2012). Spectroscopic (FT-IR, FT-Raman, UV and NMR) investigation and NLO, HOMO–LUMO, NBO analysis of organic 2,4,5-trichloroaniline. Spectrochim Acta A. 97:321-245.

Grebenkin SY, Bolshakov BV (1999). Cage effects upon light irradiation on azo compounds: cis→trans isomerization in polymethyl methacrylate J. Photochem. Photobiol. A: Chem. 122:205-209.

Kalinowski HO, Berger S, Braun S (1988). Carbon-13 NMR spectroscopy, John Wiley and Sons, Chichester.

Karakurt T, Dinçer M, Çukurovalı A, Yılmaz I (2012). Ab initio and semi-empiricalcomputational studies on 5-hydroxy-5,6-di-pyridin-2-yl-4,5-dihidro-2H-[1,2,4]triazine-3-thione J. Mol. Struct. 1024:176–188.

Kayitha E, Sundaraganesan N, Sebastian S (2010). Molecular structure, vibrational spectroscopic and HOMO, LUMO studies of 4-nitroniline by density functional method. Indian J. Pure. Appl. Phys. 48:20-30.

Nataraj A, Balachandran V, Karthick T (2013). Molecular orbital studies (hardness, chemical potential, electrophilicity,and first electron excitation), vibrational investigation and theoretical NBOanalysis of 2-hydroxy-5-bromobenzaldehyde by density functional method. J. Mol. Struct. 2031:221-233.

Koopmans T (1934). Ordering of wave functions and eigenvalues to the individual electrons of an atom, Physica. 1:104-113.

Palafox MA, Tardajos G, Martines AG, Rastogi VK, Mishra D, Ojha SP, Kiefer W (2007). FT-IR, FT-Raman spectra, density functional computations of the vibrational spectra and molecular geometry of biomolecule 5-aminouracil. Chem. Phys. 340:17-31.

Parr RG, Szentpaly L, Liu S (1999). Electrophilicity Index, J. Am. Chem. Soc. 121:1922-1924.

Pavia DL, Lampman GM, Kriz GS, Engel RG (1998). Introduction to organic laboratory techniques. W.W. Norton & Company. New York.

Pearson RG (1993). The principle of maximum hardness, Acc. Chem. Res. 26:250-255.

Perdew JP, Ernzerhof M, Burke K (1996). Rationale for mixing exact exchange with density functional approximations J. Chem. Phys. 105:9982-9986.

Perez M, Part MD, Beltran JL (2000). Determination of sulphonate dyes in water by ion-interaction high-performance liquid chromatography. J. Chromatogr A, 871:227-234.

Pihlaja K, Kleinpeter E (1994). Carbon-13 Chemical Shifts in Structural and Stero-Chemical Analysis, VCH Publishers, Deerfield Beach.

Rastogi VK, Singhal S, Palafox MA, Ramana Rao G (2010). Vibrational spectra, normal coordinate analysis and thermodynamics of 2, 5-difluorobenzonitrile Indian J. Phys. 84:151-165.

Silverstein M, Basseler GC, Morill C (1981). Spectrometric Identification of Organic compounds, Wiley, New York.

Tamai N, Miasaka H (2000). Ultrafast Dynamics of Photochromic Systems. Chem. Rev. 100: 1875 -1890.

Tarcan E, Pekparlak A, Avcı D, Atalay Y (2009). Theoretical studies of molecular structure And vibrational spectra of the asymmetric Squaraine [(2-dimethylamino-4-anilino) Squaraine] Arabian J. Sci. Engr. 2A. 34:55-62.

Teimouri A, Chermahini AN, Emami M (2008). Synthesis, characterization, and DFT studies of a novel azo dye derived from racemic or optically active binaphthol. Tetrahedron. 64:11776–11782.

Usha RA, Sundaraganesan N, Kurt G, Cinar M, Karabacak M (2010). FT-IR, FT-Raman, NMR spectra and DFT calculations on 4-chloro-N-methylaniline. Spectrochim Acta A 75:1523–1529.

Varsányi G, Sohár P, (1972) Infrared spectra of 1,2,3,5-tetra-. substituted benzene derivatives, I. Acta Chim. Acad. Sci. Hung., 74: 315-333.

Varsanyi G. (1969) Vibrational Spectra of Benzene Derivatives, Academic Press, New York.

Yang S, Tian H, Xiao H, Shang X, Gong X, Yao S, Chen K (2001). Photodegradation of cyanine and merocyanine dyes . Dyes and Pigments. 49:93–101.

Yazıcı S, Albayrak C, Gümrükçüoglu I, Senel I, Büyükgüngör O (2011). Experimental and density functional theory (DFT) studies on (E)-2-Acetyl-4-(4-nitrophenyldiazenyl) phenol. J. Mol. Struct. 985:292-298.

Zhang R, Dub B, Sun G, Sun Y (2010). Experimental and theoretical studies on o-, m- and p-chlorobenzylideneaminoantipyrines. Spectrochim Acta, 75A:1115-1124.

Zhou Z, Navangul HV (1990). Absolute hardness and aromatisity: MNDO study of benzenoid hydrocarbons, J. Phys. Org. Chem. 3:784-788.

Zollinger H (1987). Colour Chemistry: Synthesis, properties and application of organic dyes and pigments. VCH. New York.

academicJournals

Vol. 8(29), pp. 1506-1514, 9 August, 2013
DOI: 10.5897/IJPS12.624
ISSN 1992 - 1950 © 2013 Academic Journals
http://www.academicjournals.org/IJPS

International Journal of Physical Sciences

Full Length Research Paper

Evaluation of extraction methods for the analysis of selected polybrominated diphenyl ethers and hexabromobiphenyl (BB-153) – application to aqueous environmental samples

Daso, Adegbenro P.[1,3,*], Fatoki, Olalekan S.[2] and Odendaal, James P.[1]

[1]Department of Environmental and Occupational Studies, Faculty of Applied Sciences, Cape Peninsula University of Technology, Cape Town, South Africa.
[2]Department of Chemistry, Faculty of Applied Sciences, Cape Peninsula University of Technology, Cape Town, South Africa.
[3]Department of Food and Agricultural Sciences, Faculty of Applied Sciences, Cape Peninsula University of Technology, Cape Town, South Africa.

Accepted 30 July, 2013

The increasing evidence of the presence of organic pollutants in different aqueous matrices has led to the development of many analytical techniques. The isolation of these compounds from the aqueous matrices remains an integral component of these techniques. In this study, the performance of three different extraction methods, namely separatory funnel, magnetic stirring and solid-phase extraction methods commonly applied to organic pollutants in aqueous matrices was assessed. The extraction efficiencies of the target compounds BDE 28, 47, 100, 99, 154, 153 and 183 as well as BB 153 were evaluated using spiking experiments. More so, the performance of a modified clean-up technique was compared with the conventional glass column chromatographic technique. The results from these studies showed that the separatory funnel extraction technique gave the best recoveries. The percent recoveries of these compounds ranged from 72 to 89%, 65 to 84% and 26 to 122% for the separatory funnel, magnetic stirring and solid-phase techniques, respectively. The modified clean-up technique, which requires the use of fewer quantities of the adsorbent material and eluting solvent, gave comparable results with the conventional column technique. The combination of the best extraction method and the modified clean-up techniques was applied to different aqueous matrices, including river water, wastewater treatment effluent and landfill leachate samples.

Key words: Polybrominated diphenyl ethers (PBDEs), landfill leachate, effluent, river water, black river, Cape Town.

INTRODUCTION

Brominated flame-retardants (BFRs) have been used for many years in a wide variety of commercial products, including furniture, plastics, computers and electronics. Their mechanism of action involves the release of free bromine radicals when heated. These free radicals, in turn, scavenge other free radicals taking part in the flame

*Corresponding author. E-mail: adegbenrop@yahoo.com.

propagation, thus resulting in continuous flame retardation process (Richardson, 2009). Although, the use of these chemicals has drastically reduced the incidences of fire-related deaths, injuries and property damage, there is still growing concerns about their widespread distribution in the environment.

Polybrominated diphenyl ethers (PBDEs) represent important category of additive brominated flame-retardants. Their global demand has increased significantly since the use of polybrominated biphenyls (PBBs) was banned a few decades ago. The commercial formulations of PBDEs include three main categories, namely Penta- (consisting primarily of BDEs 47 and 99, alongside other congeners of tri- hepta-BDEs), Octa- (hexa – deca-BDEs – the exact congener composition of this group vary considerably between the two principal formulations marketed) and Deca- (92 to 97% BDE-209 plus nona- and octa-BDEs) (La Guardia et al., 2006). Typical quantities of these chemicals in products may reach up to 18% for pentabrominated diphenyl ethers (penta-BDEs), 15% for octabrominated diphenyl ethers (octa-BDEs) and 16% for decabrominated diphenyl ethers (deca-BDEs) (Alaee et al., 2003). Owing to the quantity of these chemicals present in products of everyday use and their mode of incorporation into polymeric materials, which is, additive in nature, the tendency for these chemicals to leach out of the treated products during their usage and disposal is highly probable. Consequently, increasing levels of these contaminants have been reported globally in different environmental matrices.

PBDEs have been detected in soil (Jiang et al., 2010; Zheng et al., 2012; Parolini et al., 2013), sediment (Klosterhaus et al., 2012; Moon et al., 2012), sewage sludge (Gevao et al., 2008; Yang et al., 2011; Cincinelli et al., 2012; Xiang et al., 2013), indoor dust (Takigami et al., 2009; Ali et al., 2011; Kang et al., 2011; Coakley et al., 2013), in foodstuffs (Bocio et al., 2003; Gomara et al., 2006; Schecter et al., 2008; Luo et al., 2009) and in aquatic and terrestrial wildlife (Polder et al., 2008; Cheaib et al., 2009). PBDEs have also been detected in human milk, adipose tissue, serum, hair and placenta, particularly in subjects who are occupationally exposed (Sudaryanto et al., 2008; Zhao et al., 2008, 2009; Zhu et al., 2009; Eguchi et al., 2012). Unfortunately, the investigation of these contaminants in aqueous environmental samples has not received the required attention. This might probably be due to the unique physico-chemical properties of these chemicals. PBDEs, like most organic pollutants, are highly hydrophobic, thus exhibiting extremely low solubility, low vapour pressure and high octanol – water co-efficient (de Wit, 2002). Given these properties, it is expected that their ultimate fate in aqueous media will be greatly influenced by the presence of suspended particulate matter (Ramu et al., 2010). Hence, it might be needful to carefully select extraction methods that can produce acceptable recoveries of the target compounds.

Aqueous environmental samples derived from different industrial processes as well as from waste treatment facilities (WWTPs and landfill sites) often contain high loads of these emerging contaminants. Inadequate treatment of these waste streams may, therefore, contribute significantly to further contamination of the receiving environment. The development of an appropriate analytical procedure for the isolation (extraction) of these contaminants is very critical to evaluating their levels in various aqueous matrices. Until now, organic contaminants in aqueous matrices are traditionally isolated using liquid-liquid extraction technique. Although, newer techniques have been developed and applied for the analysis of various organic pollutants, including PBDEs. These include ultrasound-assisted emulsification micro-extraction (Fontana et al., 2009), solid phase micro-extraction (Wang et al., 2006) and so on. These techniques, however, have not found wide applicability in the analysis of PBDEs, particularly in aqueous samples.

The aim of this present study was to evaluate the efficiencies of three methods of extraction commonly applied to the analysis of organic pollutants with a view to identify the best extraction technique for the analysis of selected PBDE congeners as well as BB 153 in aqueous samples. Furthermore, the study also attempts to determine the levels of these pollutants in different aqueous samples, including wastewater effluents, landfill leachate as well as river water collected within the city of Cape Town.

MATERIALS AND METHODS

Chemicals and materials

All organic solvents (n-hexane, dichloromethane, acetone and isooctane) purchased from Merck (Modderfontein, South Africa) were doubly-distilled prior to use. Anhydrous sodium sulphate was purchased from Radchem (Pty) Ltd. (Roodepoort West (Gauteng), South Africa). Silica gel (60 – 200 mm) and copper powder were supplied by Sigma-Aldrich (Aston Manon (Gauteng), South Africa). High purity gases (helium – 99.999%; nitrogen 99.999%) were purchased from by Afrox (Pty) Ltd. (Cape Town, South Africa). Unlabelled individual reference PBDEs standards were produced by Cambridge Isotope Laboratories (CIL) (Andover, MA, USA). BB 153 was produced by Chiron AS (Trondheim, Norway). These standards were locally supplied by Industrial Analytical (Pty) (Midrand (Gauteng), South Africa).

Sample collection, extraction and clean-up procedures

Aqueous samples, including river water, WWTP effluents and landfill leachate were collected between April and May, 2010. River water samples collected correspond to the upstream, point of discharge and downstream sampling points of the effluent-receiving Black River in the city of Cape Town. Effluent samples from a nearby WWTP were collected at different stages of the wastewater purification process, namely: inlet section (raw water); primary settling tank (primary effluent); secondary settling tank (secondary

effluent) and disinfection unit (final effluent). The raw leachate samples were collected from the leachate reservoir sited on-site. Depending on its level in this reservoir, leachate is periodically pumped into the nearby WWTP for treatment. All these samples were collected in triplicates into thoroughly cleaned 1 L amber glass bottles with amber glass caps. The samples were kept cool *en-route* the laboratory in an ice container. Samples were immediately refrigerated on arrival at the laboratory at 4°C until analysis.

Three extraction methods, namely: separatory funnel extraction (SFE), magnetic stirring extraction (MSE) and solid-phase extraction (SPE) methods were investigated in this study. For this purpose, a known volume of ultra-pure MilliQ water (RiOs8^{TM}, France) was spiked with standard mixture of all target compounds to be investigated. The extraction of these compounds was carried out by employing each of the methods to be evaluated. The overall recoveries of these compounds were subsequently estimated. The method that gave the best analytes' recoveries was applied to the analysis of aqueous samples investigated in this study. The detailed procedure for each extraction method is described below.

Separatory funnel extraction method

About 800 ml of MilliQ water was measured into a thoroughly cleaned 1 L capacity separatory funnel. The water was thereafter spiked with 1 ml of standard solution containing all the target compounds. The set up was allowed to equilibrate for exactly 60 min before extraction. Analytes extraction was carried out by shaking the spiked water with 40 ml of dichloromethane for 2 min with periodic venting during the extraction. Phase separation of the two layers that results was allowed to take place for about 10 to 15 min. The lower organic layer was thereafter collected over anhydrous sodium sulphate into a 250 ml-capacity round bottom flask. The extraction of aqueous layer was repeated twice using 40 ml of dichloromethane in each occasion. The separatory funnel was rinsed twice with 20 and 10 ml of dichloromethane in succession after the aqueous layer had been discarded. These were combined with the extract previously obtained. The extract obtained was concentrated using a rotary evaporator at 45°C to about 1 ml.

Magnetic stirring extraction method

Similarly, 800 ml of MilliQ was water measured into a thoroughly cleaned 2 L capacity beaker. The water was spiked and allowed to equilibrate as previously described for the separatory funnel technique. In contrast to the SFE technique, however, the analytes were extracted once using a total of 120 ml dichloromethane with moderately rigorous stirring for 30 min by employing a magnetic stirrer (FMH Electronics, South Africa). The phase separation of both aqueous and organic layers was allowed to take place for about 30 min. The clear supernatant was thereafter decanted and the bottom layer was transferred into a clean 500 ml capacity separatory funnel for further phase separation. The lower organic layer was then collected over anhydrous sodium sulphate into a pre-cleaned 250 ml capacity round-bottom flask. The beaker and separatory funnel used were rinsed with 20 and 10 ml of dichloromethane in succession and were combined with the extract previously obtained. The extract obtained was thereafter concentrated to about 1 ml using a rotary evaporator.

Solid-phase extraction method

This extraction method began with the initial conditioning of the C-18 cartridges employed. This was done by passing 5 ml of n-hexane, 5 ml of dichloromethane, 5 ml of methanol and 5 ml of MilliQ water in succession through the cartridge at low pressure (1.5 in Hg) employing a Visiprep manifold (Sigma-Aldrich). To investigate the influence of pH of the aqueous matrices on the recovery of target analytes using SPE cartridges, two different set-ups, including those with pH adjustment and the other without pH adjustment were investigated. First, the set-up with pH adjustment had its pH adjusted to between 2.05 and 2.12 using conc. H_2SO_4 (98% purity). This was done by adding the acid in a drop wise manner followed by regular stirring and prompt measurement of the pH with a pH meter until the desired pH was attained. The pH of the other set-up was unaltered and these values ranged between 7.28 and 7.69. These set-ups were allowed to equilibrate for 60 min after each had been spiked with 1 ml of standard solution containing all the target compounds. Each of the spiked MilliQ water was then extracted by passing it through the pre-conditioned cartridge at a pressure of 10 in Hg. Upon completion of the extraction, the cartridges were vacuum dried for an additional 45 min. The analytes were, thereafter, eluted with 6 ml n-hexane: dichloromethane (1:2) at a pressure of 1.0 in Hg with an average flow of 1 drop per 10 s. The eluate was subsequently spiked with 300 µl of iso-octane and concentrated under a gentle stream of nitrogen gas to a suitable volume. The extract was then quantitatively transferred into amber samples for instrumental analysis.

Extract clean up procedure

In this case, two clean-up procedures were employed. These column chromatographic techniques involved the use of varying quantities and forms of silica gel packed in Pasteur pipette and glass column for the modified and conventional techniques, respectively. More so, different volumes of the eluting solvent were tested for both techniques to obtain the optimum volume that will yield the best recoveries of the target compounds. For the modified clean-up technique, 5 and 10 ml of the eluting solvent were tested, whereas 25, 50, 75, 100 and 125 ml of the eluting solvent were tested for the conventional glass column technique.

The Pasteur pipette packing was done by first clogging its tip with a clean glass wool. This was followed by the addition of 0.1 g activated silica gel; 0.2 g (30% 1N NaOH, w/w) basic silica gel; 0.1 g activated silica gel; 0.4 g (44% conc. H_2SO_4, w/w) acidic silica gel; 0.1 g activated silica gel; 1.0 g anhydrous sodium sulphate) in this sequence from the bottom. The packed column was, thereafter, conditioned with 5 ml of n-hexane. Similarly, the glass column was packed from the bottom with 1 g activated silica gel (previously baked at 240°C overnight), 4 g basic silica gel (30% NaOH, w/w), 1 g activated silica gel, 8 g acidic silica gel (44% conc. H_2SO_4, w/w), 2 g activated silica gel and 4 g anhydrous sodium sulphate. Basically, this clean-up procedure was done in accordance with the USEPA Draft Method 1614 for the analysis of PBDEs in wastewater and bio-solids, although, certain aspects of the regulatory procedure were modified.

The packed column was pre-conditioned with 50 ml of doubly distilled n-hexane to remove trapped air and background contaminants within the column. The n-hexane layer over the uppermost layer in the column was maintained at 2 mm to prevent further infiltration of air into the column. The concentrated extract in n-hexane was then quantitatively transferred into the column and eluted with appropriate volume of the eluting solvent. The eluate was further concentrated using a rotary evaporator to about 1 ml. The concentrated cleaned extract was the spiked with about 300 µl of iso-octane before the final concentration was done under a gentle stream of nitrogen gas. The prepared samples were stored in amber sample vials and kept in the refrigerator until the final instrumental analysis.

Instrumental analysis

The analysis of the target compounds was performed using an

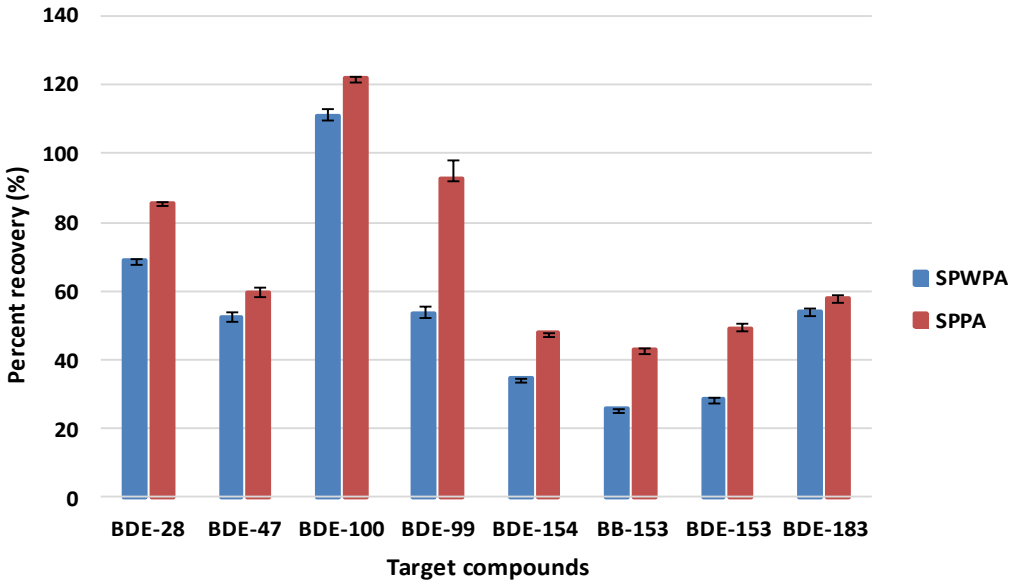

Figure 1. Influence of pH adjustment on the recovery of target compounds (SPWPA – solid phase extraction without pH adjustment; SPPA –solid phase extraction with pH adjustment; error bars represent standard deviations of 3 replicates).

Agilent 6890 gas chromatograph equipped with electron capture detector (GC-µECD). The GC-µECD was equipped with an Agilent 7890B autosampler. Chromatographic separation of analytes was performed using a DB-5 MS column (60 m length, 0.25 mm i.d. and 0.1 µm film thickness). Helium gas was employed as the carrier gas with a flow rate of 1.5 ml/min using a constant flow mode. High purity nitrogen gas was used as a make-up gas for the detector at a flow rate of 30 ml/min. The injector and detector temperatures were set at 280 and 300°C, respectively. The oven temperature was programmed as follows: 100°C held for 2 min, ramped at 20°C/min to 220°C; it was further ramped at 4°C/min to 300°C and held for 7 min. One micro-litre of either the standard mixture or experimental samples was injected using a splitless injection mode. Quantification was based on peak areas of target compounds using external calibration technique. Five to six calibration levels containing 1, 5, 10, 25, 50 and 100 ng/ml for all target compounds except BDE-183 which had a calibration level of 5, 10, 25, 50 and 100 ng/ml. The identification of the target analytes in the real samples was done by comparing their retention times with those of the reference standards.

For quality control and assurance purposes, the retention times of target analytes were only considered if they fall within 5% interval relative to those of the reference standards. A procedural blank (MilliQ water) was run with the batch of 5 field samples. No detectable level of analytes was found. In addition, a calibration standard of 10 ng/ml was run as a check after every 5 samples to ensure that less than 20% variation was found from the initial calibration standards. All data were processed with Microsoft Excel software (2007 version).

RESULTS AND DISCUSSION

The influence of pH adjustment on analytes recovery using SPE technique

The recoveries of certain organic compounds were generally enhanced when the pH of the medium in which they were found was lowered. This assumption has been found to be generally true for ionisable organic compounds such as phenols and aniline (Yang et al., 2008). Although, PBDEs are non-ionisable compounds, this phenomenon was investigated for the selected compounds at a pH range between 2.05 and 2.12 using solid phase extraction technique. The recoveries obtained for the highly brominated congeners on SPE cartridges were generally poor. Only a slight increase in the yield of all target compounds was observed for the experimental set-ups whose pH had been adjusted (Figure 1). The observed differences in the recoveries of the lower and higher PBDE congeners could be attributed to the relatively lower polarity of the higher brominated congeners (Eljarrat et al., 2004). Other possibility could result from the ability of the sorbent materials in the SPE cartridges to demonstrate stronger affinity for PBDEs at lower pH than at neutral pH levels; thus, resulting in a slight yield in PBDEs recovery upon elution with the appropriate solvent.

Evaluation of extraction efficiencies of different methods

A critical evaluation of the efficiencies of different extraction methods studied revealed that the isolation of target compounds from the aqueous medium assumed different patterns. With the use of C-18 cartridges, the recoveries of target compounds were generally poor when compared with other extraction techniques. However, the choice of solvent or solvent combinations

Table 1. Percent recoveries of target compounds obtained from different extraction techniques.

	SFM		MSM		SPWPA		SPPA	
Target compounds	**Spiked concentration (ng/ml)**	**Concentration recovered (ng/ml)**	**% Recovery**	**Concentration recovered (ng/ml)**	**% Recovery**	**Concentration recovered (ng/ml)**	**% Recovery**	**Concentration recovered (ng/ml)**	**% Recovery**
BDE 28	10	7.94±0.13[a]	79.4	8.14±0.19[a]	81.4	6.89±0.43	68.9	8.58±0.21	85.8
BDE 47	10	8.93±0.35	89.3	8.41±0.22	84.1	5.23±1.77	52.3	5.97±1.62	59.7
BDE 100	10	7.36±0.93	73.6	6.47±1.05	64.7	11.1±2.19	111	12.2±0.55	122
BDE 99	10	8.41±0.27	84.1	7.24±0.42	72.5	5.35±2.26	53.5	9.30±5.37	93.0
BDE 154	10	7.80±0.40	78.0	7.21±0.51	72.1	3.45±0.15	34.5	4.79±0.12	47.9
BB 153	10	7.16±0.53	71.6	6.50±0.43	65.0	2.57±0.21	25.7	4.32±0.30	43.2
BDE 153	10	8.18±0.51	81.8	7.29±0.71	72.9	2.86±0.56	28.6	4.93±1.31	49.3
BDE 183	10	7.81±2.38	78.1	7.78±1.22	77.8	5.40±0.98	54.0	5.78±1.48	57.8

[a] – values represent mean (±standard deviation) of six replicates and three replicates for SPWPA and SPPA; SFM – separatory funnel extraction method; MSM – magnetic stirring extraction method; SPWPA – solid phase extraction without pH adjustment; SPPA – solid phase extraction with pH adjustment.

employed for elution is believed to play a vital role in their isolation. In this study, a significant difference in the yield of target compounds was observed when different solvent combinations were employed. During the preliminary studies, a relatively higher recovery was found when the target compounds were eluted with 6 mℓ n-hexane-dichloromethane (1:2, v/v) than when similar volume of n-hexane-acetone (2:1, v/v) was used (data not included). Notwithstanding the limitations of this method, it still offers numerous advantages, including high sample throughput, automation compatibility, reduced organic solvent consumption and excellent separation of interfering species. Additionally, the use of SPE cartridges is advantageous, as it does not often require further clean up step like other extraction techniques, thus resulting in shorter analysis time.

Despite the introduction of modern extraction methods, liquid-liquid extraction techniques still find extensive application in the analysis of organic contaminants in aqueous samples. Separatory funnel and magnetic stirring methods represent important category of this technique that are still being used extensively. These methods were included in this study due to their wide applicability to other organic pollutants. Most of the methods selected for evaluation have either been employed for the assessment of PBDEs or other similar contaminants such as PCBs, organochlorine pesticides, phenols, amongst others, in aqueous matrices (Pauwels et al., 1999; Covaci and Schepens, 2001).

The results indicating the extraction efficiency of each of these methods are presented in Table 1. Based on these findings, it was apparent that the separatory funnel method had the best extraction efficiency for most of the congeners investigated. Although a good recovery of these congeners was also achieved with the magnetic stirring method, the majority of the congeners were efficiently isolated with the separatory funnel method.

Both methods employ dispersion of fine droplets generated by the agitation of the aqueous samples present in the extraction chamber. The isolation of the compounds of interest is, therefore, achieved with the continuous contact maintained between the aqueous and organic droplets within the chamber.

In contrast, the solid-phase method effects the extraction of these compounds through adsorption mechanism. Essentially, this method explores the differential affinities of components present in the aqueous matrix to effect the isolation or purification of the desired compounds (Rouessac and Rouessac, 2007). Besides the numerous advantages this technique offers, which include ease of automation, higher recoveries of polar compounds and cleaner extracts, certain problems are still associated with the use of this method. These include incomplete removal of interferences, low recovery of analytes and high degree of variability in terms of relative standard deviation (RSD).

The recoveries of PBDEs as well as BB 153 employing this method were generally low. A

Table 2. Mean percent recovery of target compounds with the conventional glass column clean up technique.

Target compounds	Percent recovery (%) volume of eluting solvent				
	25 ml	50 ml	75 ml	100 ml	125 ml
BDE 28	-	7.11	92.9	95.2	95.9
BDE 47	-	12.4	94.0	95.7	97.1
BDE 100	-	66.0	94.6	97.4	98.5
BDE 99	-	47.9	96.3	99.3	101
BDE 154	-	70.1	93.7	100	101
BB 153	-	82.8	100	100	104
BDE 153	-	68.8	97.1	103	104
BDE 183	-	71.7	93.2	95.9	98.8

– not detected.

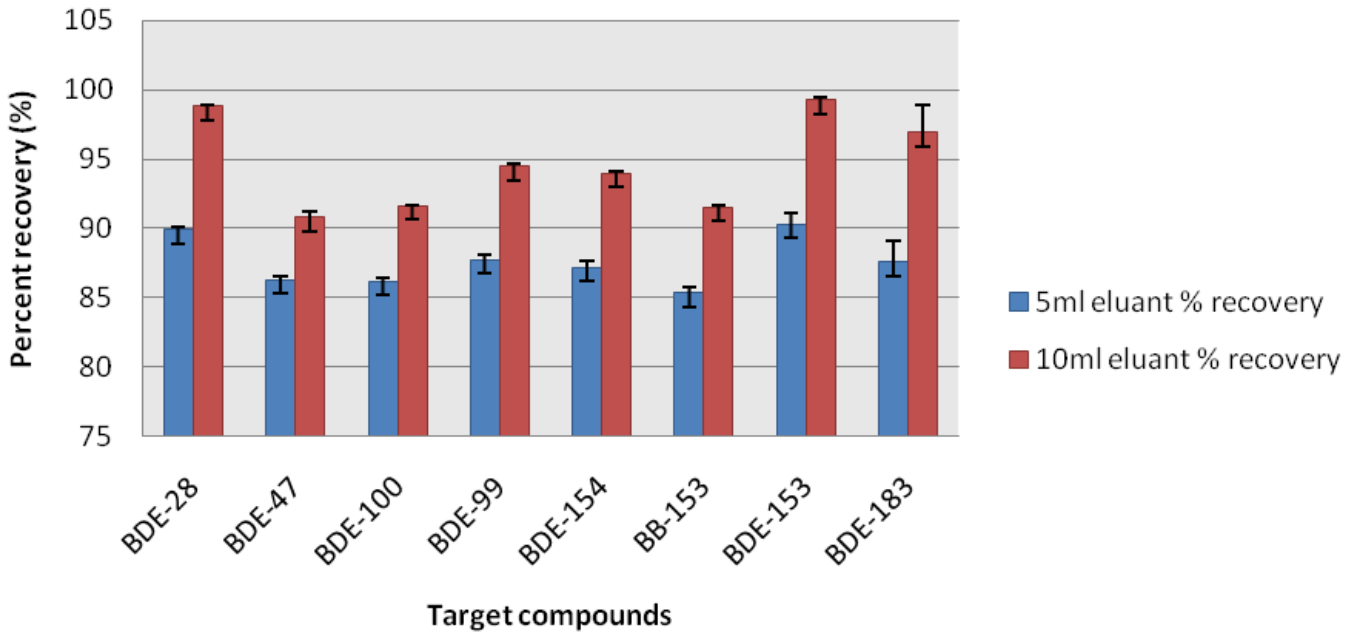

Figure 2. Percent recovery of target compounds using different eluting volumes on modified clean up technique.

slight improvement in the extraction efficiency was observed when the pH of the aqueous medium was adjusted as shown in Figure 1. It therefore implies that the recovery of these contaminants could be enhanced by simply acidifying the aqueous medium containing them if SPE technique is to be employed for their extraction. Another aspect where certain modifications were carried out during the method development was in the clean up procedure. While the conventional silica gel column chromatography was used for the purification of the sewage sludge extracts, a modified clean up technique was employed for the extracts of bottom sediment and aqueous samples investigated in this study.

For environmental monitoring studies that involve the analysis of several samples, the development and application of appropriate analytical protocols that will ensure minimal usage of both eluting solvent and adsorbent materials are highly essential. Consequently, the use of Pasteur pipette packed with different forms of silica gel for “clean-up” ensured that this objective was achieved. In this study, an attempt was made to compare the efficiency of the modified Pasteur pipette technique with the conventional glass column method. During the preliminary studies, both techniques were optimised using varying volumes of the eluting solvent. This measure was undertaken to establish the optimum volume of the eluting solvent required for both techniques. The outcomes of these investigations are presented in Table 2 and Figure 2.

Figure 2 shows the recovery of target analytes using the modified technique. With this approach, a yield greater than 85% was achieved with the use of 5 ml of the eluting solvent. Recoveries comparable to those

Table 3. Mean (standard deviation) concentrations (ng/L) of target compounds in different aqueous matrices investigated.

Target compounds	River water			WWTP Effluent				Landfill site
	Upstream	Point of discharge	Downstream	Raw water	Primary effluent	Secondary effluent	Final effluent	Leachate
BDE 28	180 (29.9)	136 (28.6)	17.4 (9.06)	10.5 (8.06)	0.73 (0.59)	12.5 (9.31)	9.66 (3.31)	1.21 (1.10)
BDE 47	29.5 (6.58)	17.9 (13.7)	8.12 (2.58)	7.45 (2.30)	4.21 (2.82)	15.1 (3.91)	16.8 (6.71)	8.97 (0.72)
BDE 100	12.1 (5.64)	7.57 (3.39)	6.31 (1.50)	1.65 (1.97)	0.19 (0.13)	5.20 (2.10)	7.34 (3.44)	0.24 (0.49)
BDE 99	7.54 (3.55)	4.93 (4.00)	3.32 (2.33)	3.64 (2.55)	2.31 (1.29)	6.57 (3.20)	6.03 (3.64)	0.00 (0.00)
BDE 154	1.67 (2.59)	0.83 (0.96)	1.75 (1.04)	0.00 (0.00)	0.64 (0.84)	1.47 (2.52)	2.12 (2.77)	0.00 (0.00)
BB 153	1.63 (1.71)	2.21 (1.10)	1.55 (0.48)	0.29 (0.72)	0.00 (0.00)	0.53 (0.70)	2.07 (1.46)	0.00 (0.00)
BDE 153	3.54 (3.14)	8.03 (2.94)	28.7 (11.9)	62.4 (42.9)	7.52 (5.91)	81.6 (40.6)	141 (62.1)	0.56 (1.11)
BDE 183	11.2 (18.2)	46.5 (43.7)	41.5 (26.0)	19.7 (14.9)	1.55 (3.10)	17.3 (5.46)	13.9 (7.36)	0.00 (0.00)

obtained with 125 ml of the eluting solvent in the conventional glass column technique were achieved when 10 ml of the eluting solvent was employed in the modified clean-up technique. With these modification measures, the conservation of up to 92% of the eluting solvent and 88% of the sorbent materials was achieved relative to the conventional glass column chromatographic technique investigated in this study. Although the modified technique proved to offer improved separation of analytes, fast and cost-effective, its major setback was decreased efficiency with the age of the sorbent materials employed. Consequently, the use of freshly prepared sorbents must be employed in order to obtain acceptable results.

Analysis of real aqueous samples

The extraction of real samples was carried out with the separatory funnel extraction method since it gave the best recoveries of all the target compounds investigated. Similarly, the purification of the extracts obtained from these samples was performed using the modified Pasteur pipette clean-up technique. The results obtained for the analysis of these samples are presented in Table 3. It was apparent that higher levels of the target compounds, especially the lower brominated congeners were detected in the upstream samples than in the other sampling points. This trend is not so surprising as there are several activities taking place around the sampling point that could possibly contribute to the observed levels. First, a few metres away from the upstream sampling point is situated the city's largest solid waste transfer station. Several thousands of tonnes of solid waste materials are received on a daily basis, which are further transferred to designated landfill sites within the city. The inter-related activities associated with the solid waste handling and disposal could contribute to the trend observed in this study.

Secondly, the Black River has been and is still an important channel through which other tributaries empty their contents. Most of these tributaries convey discharges from WWTPs, storm water run-off, agricultural run-off as well as grey water from informal settlement. The imminent variations in the composition of these notable point and non-point sources from time to time could ultimately influence the influx of the target compound in the receiving water bodies. For instance, grey water is known to contain and transport considerable amount of organic pollutants, including PBDEs (Donner et al., 2010). As observed in this study, varying levels of the target compounds were detected at different sampling points along the stretch of the investigated river. Generally, relatively low levels of the target compounds were detected at the downstream sampling point as compared with other sampling points. It is a possibility that the discharge of treated effluent from the nearby WWTP is producing dilution effects, thus resulting in the lower levels being detected. The trends assumed by the target compounds across the different sampling units within the WWTP investigated were generally inconsistent. It was, however, obvious that there were significant decreases in contaminants' levels as the waste stream flow from the inlet section into the primary sedimentation tanks. Surprisingly, the general decrease in contaminants' levels did not follow

the expected trend in both the secondary sedimentation tanks and the final effluent. In this case, a somewhat higher level of these contaminants were detected in the final effluent than in the secondary effluent. A common problem associated with most WWTPs is over-loading or over-stretching of plant's treatment capacity. Excessive loading of treatment plant could result in shorter residence time of the aqueous waste stream. The resultant effects are excessive accumulation of contaminants and poor effluent quality evidenced by the high variability in the levels of contaminants detected within the WWTP concerned (Daso, 2011).

In this study, the mean concentrations of the target compounds were subjected to statistical correlation to establish the possible influence of WWTP discharges on the contaminants' levels detected in river water samples. The results showed there was a weak negative correlation (R^2= -0.1369) between the levels detected in the final effluent and the point of discharge water samples. However, there was a moderately strong positive relationship (R^2=0.4761) between the final effluent and the downstream water samples, thus reflecting the potential contribution of WWTP discharges to the overall contamination of the investigated river. This study further affirms the findings of a similar study where WWTP discharges is implicated as the potential source of PBDE contamination of the adjacent river (Song et al., 2006). With the exception of BDE 153, the occurrence of the target compounds were completely dominated by the lower brominated congeners in the leachate samples. In this case, BDE 47 was the most dominant congener detected in the samples. Although BB 153 was not detected in the leachate samples, its presence in river water and effluent samples indicates its high persistence in the environment.

Limitations

The focus of this study was to evaluate the efficiencies of commonly used extraction methods for PBDEs in aqueous samples. Regrettably, the matrix effects of different aqueous samples investigated in this study were not examined. Furthermore, the analysis of persistent organic contaminants, especially those containing halogens in complex environmental samples are currently being analysed with Gas chromatography–mass spectrometry (GC-MS) techniques. In this study, however, only GC-µECD was employed because the GC-MS instrument to be used could not produce satisfactory results due to its persistent instability.

Conclusion

In this study, the evaluation of different extraction and clean-up techniques was carried out. The findings showed that the liquid-liquid extraction employing separatory funnel gave the best results in terms of recoveries of all the target compounds investigated. In addition, the modified clean-up technique evaluated in this study showed comparable results with the conventional glass column chromatographic technique. The application of the modified clean-up technique for the purification of extracts obtained from aqueous matrices results in drastic reduction in the quantities of adsorbent materials and the eluting solvent employed. The separatory funnel extraction technique as well as the modified clean-up technique was applied to different aqueous matrices investigated in this study.

ACKNOWLEDGEMENTS

The authors would like to thank the National Research Foundation (NRF) for financial support and the allocation of a Grant-Holder linked D.Tech bursary to AP Daso. We also thank the Cape Peninsula University of Technology, Cape Town, South Africa for providing logistics and laboratory facilities.

REFERENCES

Alaee M, Arias P, Sjodin A, Bergman A (2003). An overview of commercially used brominated flame retardants, their applications, their use patterns in different countries/regions and possible modes of release. Environ. Int. 29:683–689.

Ali N, Harrad S, Muenhor D, Neels H, Covaci A (2011). Analytical characteristics and determination of major novel brominated flame retardants (NBFRs) in indoor dust. Analytical Bioanalytical Chem. 400(9):3073–3083.

Bocio A, Llobet JM, Domingo JL, Corbella J, Teixido A, Casas C (2003). Polybrominated diphenyl ethers (PBDEs) in foodstuffs: Human exposure through the diet. J. Agric. Food Chem. 51: 3191–3195.

Cheaib Z, Grandjean D, Kupper T, de Alencastro LF (2009). Brominated flame retardants in fish of Lake Geneva (Switzerland). Bull. Environ. Contam. Toxicol. 82:522–527.

Cincinelli A, Martellini T, Misuri L, Lanciotti E, Sweetman A, Laschi S, Palchetti I (2012). PBDEs in Italian sewage sludge and environmental risk of using sewage sludge for land application. Environ. Pollut. 161: 229-234.

Coakley JD, Harrad SJ, Goosey E, Ali N, Dirtu AC, Van den Eede N, Covaci A, Douwes J, Mannetje AT (2013). Concentrations of polybrominated diphenyl ethers in matched samples of indoor dust and breast milk in New Zealand. Environ. Int. 59:255–261.

Covaci A, Schepens P (2001). Simplified method for determination of organochlorine pollutants in human serum by solid-phase disk extraction and gas chromatography. Chemosphere. 43:439 – 447.

Daso AP (2011). The occurrence of brominated flame retardants (Polybrominated diphenyl ethers and Polybrominated biphenyls) in Cape Town environment. D.Tech Thesis. Cape Peninsula University of Technology, Cape Town, South Africa.

de Wit CA (2002). An overview of brominated flame retardants in the environment. Chemosphere, 46:583–624.

Donner E, Eriksson E, Revitt DM, Scholes L, Lützhøft HCH, Ledin A (2010). Presence and fate of priority substances in domestic greywater treatment and reuse systems. Sci. Total Environ. 408(12): 2444–2451.

Eguchi A, Nomiyama K, Devanathan G, Subramanian A, Bulbule KA, Parthasarathy P, Takahashi S, Tanabe S (2012). Different profiles of anthropogenic and naturally produced organohalogen compounds in serum from residents living near a coastal area and e-waste recycling workers in India. Environ. Int. 47:8–16.

Eljarrat E, Cal A, Barceló D (2004). Determination of decabromodiphenyl ether in sediments using selective pressurized liquid extraction followed by GC–NCI-MS. Analytical Bioanalytical Chem. 378(3):610–614.

Fontana AR, Silva MF, Martinez LD, Wuilloud RG, Altamirano JC (2009). Determination of polybrominated diphenyl ethers in water and soil samples by cloud point extraction-ultrasound-assisted back-extraction-gas-chromatography-mass spectrometry. J. Chromatogr., A. 1216:4339–4346.

Gevao B, Muzaini S, Helaleh M (2008). Occurrence and concentrations of polybrominated diphenyl ethers in sewage sludge from wastewater treatment plants in Kuwait. Chemosphere. 71:242–247.

Gomara B, Herrero L Gonzalez MJ (2006). Survey of polybrominated diphenyl ether levels in Spanish commercial foodstuffs. Environ. Sci. Technol. 40:7541–7547.

Jiang Y, Wang X, Zhu K, Wu M, Sheng G, Fu J (2010). Occurrence, compositional profiles and possible sources of polybrominated diphenyl ethers in urban soils of Shanghai, China. Chemosphere. 80: 131–136.

Kang Y, Wang HS, Cheung KC, Wong MH (2011). Polybrominated diphenyl ethers (PBDEs) in indoor dust and human hair. Atmospheric Environment 45(14):2386–2393.

Klosterhaus SL, Stapleton HM, La Guardia MJ, Greig DJ (2012). Brominated and chlorinated flame retardants in San Francisco Bay sediments and wildlife. Environ. Int. 47(0):56–65.

La Guardia MJ, Hale RC, Harvey E (2006). Detailed polybrominated diphenyl ether (PBDE) congener composition of the widely used penta-, octa-, and deca-PBDE technical flame retardants mixtures. Environ. Sci. Technol. 40:6247–6254.

Luo Y, Luo XJ, Lin Z, Chen SJ, Liu, J, Mai BX, Yang ZY (2009). Polybrominated diphenyl ethers in road and farmland soils from an e-waste recycling region in Southern China: Concentrations, source profiles, and potential dispersion and deposition. Sci. Total Environ. 407: 1105 – 1113.

Moon HB, Choi M, Yu J, Jung RH, Choi HG (2012). Contamination and potential sources of polybrominated diphenyl ethers (PBDEs) in water and sediment from the artificial Lake Shihwa, Korea. Chemosphere 88(7):837–843.

Parolini M, Guazzoni N, Comolli R, Binelli A, Tremolada P (2013). Background levels of polybrominated diphenyl ethers (PBDEs) in soils from Mount Meru area, Arusha district (Tanzania). Sci. Total Environ. 452–453(0):253–261.

Pauwels A, Wells DA, Covaci A, Schepens PJC (1999). Improved sample preparation method for selected persistent organochlorine pollutants in human serum using solid-phase disk extraction with gas chromatographic analysis. J. Chromatogr., B. 723:117–125.

Polder A, Venter B, Skaare JU, Bouwman H (2008). Polybrominated diphenyl ethers and HBCD in bird eggs of South Africa. Chemosphere. 73:148–154.

Ramu K, Isobe T, Takahashi S, Kim EY, Min BY, We SU, Tanabe S (2010). Spatial distribution of polybrominated diphenyl ethers and hexabromocyclododecanes in sediments from coastal waters of Korea. Chemosphere. 79:713–719.

Richardson SD (2009). Water analysis: Emerging contaminants and current issues. Anal. Chem. 81:4645–4677.

Rouessac F, Rouessac A (2007). Chemical analysis: Modern instrumentation methods and techniques. (2ed.). John Wiley & Sons Ltd. West Sussex, England.

Schecter A, Harris TR, Shah N, Musumba A, Papke O (2008). Brominated flame retardants in US food. Mol. Nutr. Food Res. 52:266–272.

Song M, Chu S, Letcher RJ, Seth B (2006). Fate, partitioning, and mass loading of polybrominated diphenyl ethers (PBDEs) during the treatment processing of municipal sewage. Environ. Sci. Technol. 40:6241–6246.

Sudaryanto A, Kajiwara N, Takahashi S, Tanabe SM (2008). Geogarphical distribution and accumulation features of PBDEs in human breast milk from Indonesia. Environ. Pollut. 151:130–138.

Takigami H, Suzuki G, Hirai Y, Ishikawa Y, Sunami M, Sakai S (2009). Flame retardants in indoor dust and air of a hotel in Japan. Environ. Int. 35:688–693.

Wang JX, Jiang D-Q, Gu ZY, Yan XP (2006). Multiwalled carbon nanotubes coated fibers for solid-phase microextraction of polybrominated diphenyl ethers in water and milk samples before gas chromatography with electron-capture detection. J. Chromatogr. A. 1137:8–14.

Xiang N, Zhao X, Meng XZ, Chen L (2013). Polybrominated diphenyl ethers (PBDEs) in a conventional wastewater treatment plant (WWTP) from Shanghai, the Yangtze River Delta: Implication for input source and mass loading. Sci. Total Environ. 461–462(0):391–396.

Yang C, Meng XZ, Chen L, Xia S (2011). Polybrominated diphenyl ethers in sewage sludge from Shanghai, China: Possible ecological risk applied to agricultural land. Chemosphere 85(3):418–423.

Yang K, Wu W, Jing Q, Zhu L (2008). Aqueous adsorption of aniline, phenol and their substitutes by multi-walled carbon nano-tubes. Environ. Sci. Technol. 42:7931–7936.

Zhao G, Wang Z, Dong MH, Rao K, Luo J, Wang D, Zha J, Huang S, Xu Y, Ma M (2008). PBBs, PBDEs, and PCBs levels in hair of residents around e-waste disassembly sites in Zhejiang Province, China, and their potential sources. Sci. Total Environ. 397:46–57.

Zhao G, Wang Z, Zhou H, Zhao Q (2009). Burdens of PBBs, PBDEs, and PCBs in tissues of the cancer patients in the e-waste disassembly sites in Zhejiang, China. Sci. Total Environ. 407:4831–4837.

Zheng X, Liu X, Jiang G, Wang Y, Zhang Q, Cai Y and Cong Z (2012). Distribution of PCBs and PBDEs in soils along the altitudinal gradients of Balang Mountain, the east edge of the Tibetan Plateau. Environ. Pollut. 161(0):101-106.

Zhu L, Ma B, Li J, Wu Y, Gong J (2009). Distribution of polybrominated diphenyl ethers in breast milk from North China: Implication of exposure pathways. Chemosphere. 74:1429–1434.

academicJournals

Vol. 8(29), pp. 1515-1525, 9 August, 2013
DOI: 10.5897/IJPS2013.3885
ISSN 1992 - 1950 © 2013 Academic Journals
http://www.academicjournals.org/IJPS

International Journal of Physical Sciences

Full Length Research Paper

Improved energy efficiency of photogalvanic cell with four dyes as photosensitizers in Tween 60- Ascorbic acid system

K. R. Genwa* and C. P. Sagar

Department of Chemistry, Jai Narain Vyas University, Jodhpur – 342005 India.

Accepted 30 July, 2013

The objective of this work was to increase the energy efficiency of photogalvanic cell using four dyes; Amido Black 10B, Bromocresol purple, Carmine and Biebrich scarlet as photosensitizers in Tween 60- Ascorbic acid system. Observed values of photopotential, photocurrent, fill factor, conversion efficiency and storage capacity for Tween 60 - Amido Black 10B - Ascorbic acid system were 996 mV, 420 µA, 0.38, 1.62%, 130 min, Tween 60 - Bromocresol purple - Ascorbic acid system were 811 mV, 65 µA, 0.50, 0.32%, 150 min, Tween 60 - Carmine - Ascorbic acid system were 844 mV, 190 µA, 0.43, 0.81%, 170 min. and Tween 60 - Biebrich Scarlet - Ascorbic acid system were 919mV, 210 µA, 0.41, 0.89%, 75 min, respectively. Comparative energy efficiency in all four systems studied in detail and all comparative data are discussed in the paper. Finally system with Amido black 10B and Carmine dyes was proposed as efficient system in view of solar energy conversion and storage.

Key words: Amido black 10B, bromocresol purple, carmine, biebrich scarlet, energy efficiency.

INTRODUCTION

Growing concern of rise in fossil fuel prices and environmental degradation has lead to the world's interest in renewable energy sources. Out of various renewable energy sources, solar energy is freely available and commercially viable source for electrical energy generation. The conversion of solar energy into electrical energy can be done by photoelectrochemical cells. The Photogalvanic effect was first reported by Rideal and Williams (1925) but it was systematically investigated by Rabinowitch (1940a, b). Later, various researchers reported this effect time to time (Kaneko and Yamada, 1977; Albery and Archer, 1977; Memming, 1980; Folcher and Paris, 1983; Pan et al., 1983; Naman and Karim, 1984; Jana, 2000; Ameta et al., 2006; Balzani et al., 2008; Ratcliff et al., 2011).

A new methodology of tilt angle for a solar panel to optimize solar energy extraction under cloudy conduction was reported by Armstrong and Hurley (2010). Photochemical energy conversion was studies in system containing methylene blue (Murthy and Reddy, 1979), analysis of galvano-statically synthesized polypyrole films, correlation of ionic difference and capacitance with the electrode morphology (Bisquert and Belmonte, 2002) and the molecular approaches to solar energy conversion and molecular control of interfacial charge transfer at nanocrystalline semiconductor interfaces (Meyer, 2005) were discussed.

Recently, studies on photogalvanic effect in mixed dyes and reductant systems were significantly reported (Yadav and Lal, 2010; Gangotri and Indora, 2010; Sharma et al., 2012). Some new dye-surfactant combination were studies in our laboratory in view of solar energy conversion and storage (Genwa and Kumar, 2012), but efforts are still needed to increase energy efficiency of

*Corresponding author. E-mail: krg2004@rediffmail.com. Tel: +91- 291- 2720840.

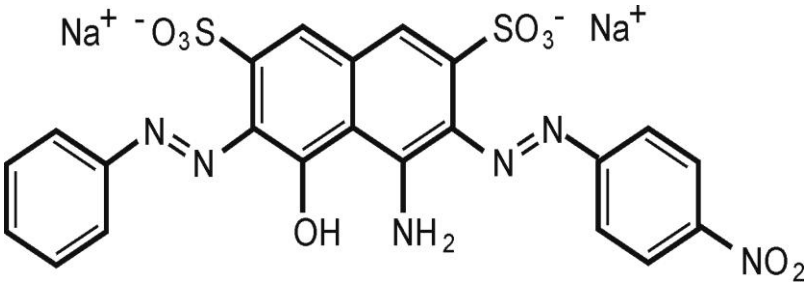

Scheme 1. Amido black 10B.

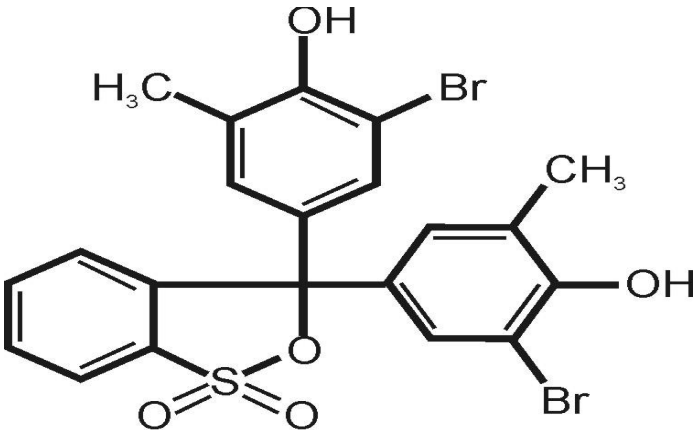

Scheme 2. Bromocresol purple.

photogalvanic cell. Therefore in this work, four dyes were selected and used as photosensitizer in photogalvanic cell to study comparative energy efficiency along with their storage performance.

MATERIALS AND METHODS

Amido black 10B

It was obtained from LOBA Chemie, Mumbai, India. Amido Black 10B (Scheme 1) is a solid crystalline black power, molecular formula $C_{22}H_{14}N_6Na_2O_9S_2$, molecular weight 616.49, soluble in water and maximum absorption (λ_{max}) 610 nm. Concentration of dye used cell solution was 1.1×10^{-5} M.

Bromocresol purple

It was obtained from LOBA Chemie, Mumbai, India. Bromocresol purple (Scheme 2) is a slightly yellow power, insoluble in water but soluble in Ethanol, molecular formula $C_{21}H_{16}Br_2O_5S$, molecular weight 540.24, and maximum absorption (λ_{max}) 580 nm . Concentration of dye used cell solution was 1.6×10^{-5} M.

Carmine

It was obtained from LOBA Chemie, Mumbai, India. Carmine (Scheme 3) is a solid red power, molecular formula is $C_{22}H_{20}O_{13}$, molecular weight is 492.39, soluble in water and maximum absorption (λ_{max}) 515 nm. Concentration of dye used cell solution was 7.2×10^{-5} M.

Biebrich scarlet

It was obtained from LOBA Chemie, Mumbai, India. Biebrich scarlet (Scheme 4) is dark red powder, soluble in water, molecular formula $C_{22}H_{14}N_4Na_2S_2$, molecular weight 556.9 and maximum absorption (λ_{max}) 520 nm. Concentration of dye used cell solution was 4.8×10^{-5} M.

Tween 60 (Polyoxyethylene sorbitan monostearate)

Tween 60 was obtained from LDH (Scheme 5) is a pale yellow semisolid liquid, soluble in water, molecular formula $C_{24}H_{46}O_6(C_2H_4O)_n$, molecular weight 1312. Concentration of Tween 60 used cell solution was 0.8 to 1.24×10^{-3} M.

Ascorbic acid

Ascorbic acid was used as reductant and it was obtained from SISCO, Mumbai, India (Scheme 6) is a white to slightly yellowish crystalline powder, soluble in water, molecular formula $C_6H_8O_6$ and molecular weight 176.13. Concentration of reductant used cell solution was 1.72 to 2.08×10^{-3} M.

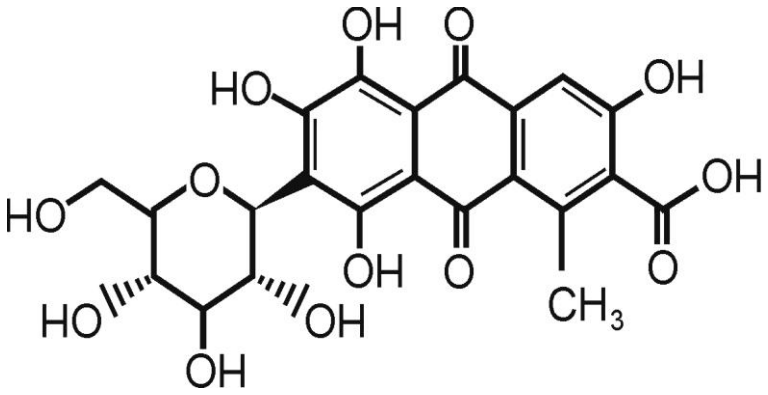

Scheme 3. Carmine.

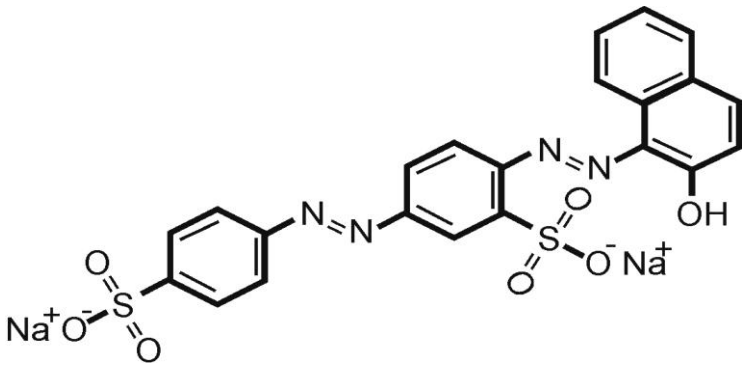

Scheme 4. Biebrich scarlet.

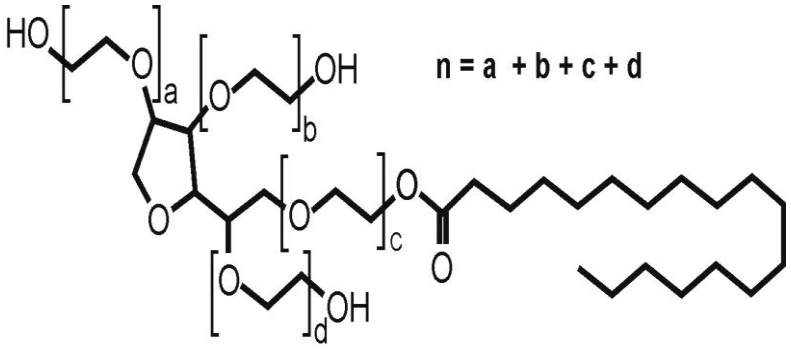

Scheme 5. Tween 60.

Photogalvanic effect of Tween 60 – Dye – Ascorbic acid systems was studied using H- shaped glass tube. Known amount of the solution of dye, reductant (ascorbic acid) and surfactant (Tween 60) was taken in the H-tube. NaOH was used to maintain the pH of solution in alkaline range. A platinum electrode (1.0 × 1.0 cm^2) was dipped in one limb and a saturated calomel electrode (SCE) immersed in another limb of the H- tube. The terminals of the electrodes were then connected to a digital pH meter (Systronics model 335, Ahmadabad, India). The entire system was first placed in dark until a stable potential was reached, then the limb containing platinum electrode was exposed to the light source (projector Tungsten lamp). The light intensity was varied by employing tungsten lamp of different wattage and measured by Solarimeter (Surya Systems, Ahmadabad). A water filter was placed between the illuminated chamber and the light source to cut off thermal radiations. The photochemical bleaching of dyes was studied potentiometrically. Absorption spectra of dye-surfactant combination have also been taken by using Spectrophotometer (Systronics 106, Ahmadabad, India) with the matched pair of silica cuvetts (path length 1 cm). All spectral measurements were

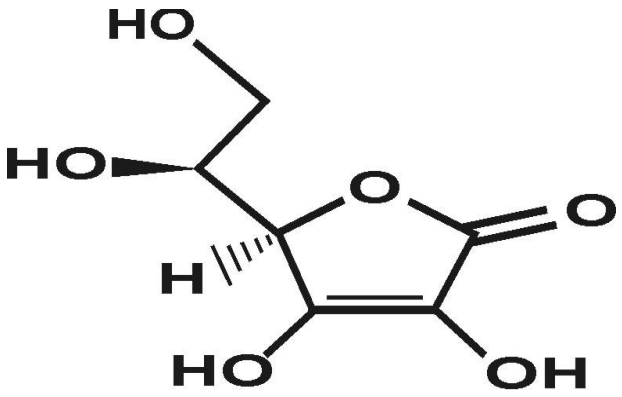

Scheme 6. Ascorbic acid.

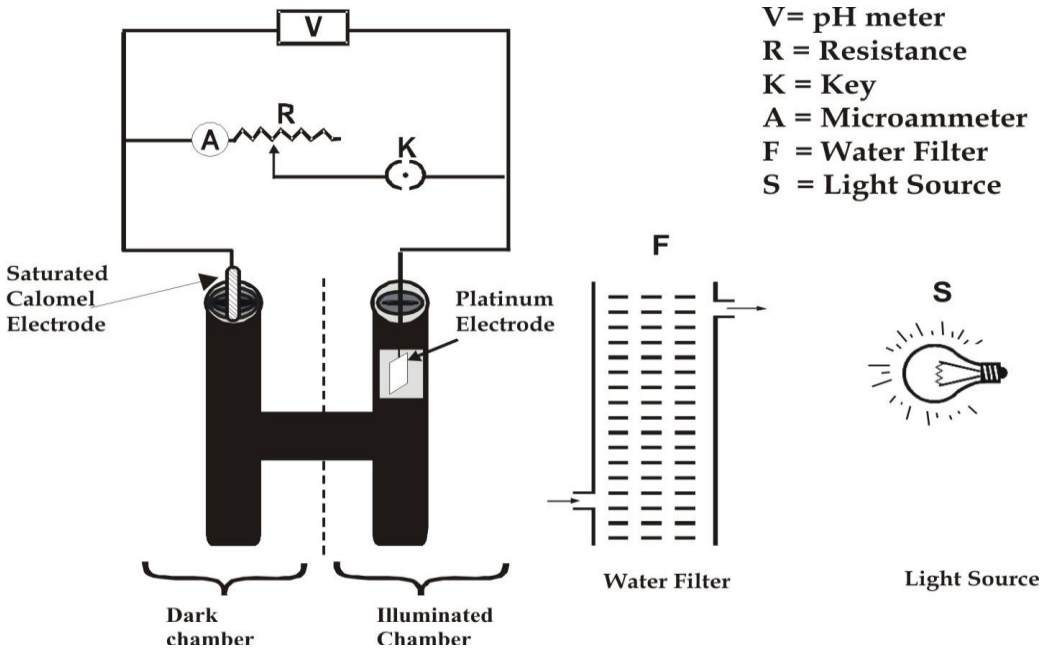

Figure 1. Set up of photogalvanic cell assembly.

duplicated in a constant temperature water bath maintained with in ±1°C and mean values were processed for data analysis. Over all experimental setup is shown in Figure 1.

RESULTS AND DISCUSSION

Effect of variation of pH

The pH of the cell solution affects the cell output in Tween 60 – Amido Black 10B – Ascorbic acid system, Tween 60 – Bromocresol purple – Ascorbic acid, Tween 60 – Carmine – Ascorbic acid and Tween 60 – Biebrich scarlet – Ascorbic acid systems. It was observed that there is an increase is in the photopotential and photocurrent with increase in pH and reaches maximum at pH 9.96 to 10.12, then on further increase in pH, photopotential and photocurrent decreased. It was further observed that these systems are sensitive to an alkaline medium and the pH for the optimum condition has a relation with pK_a of the reductant and desired pH is higher than its pK_a value ($pH>pK_a$). The reason may be the availability of reductant in its anionic form, which is better donor form. The pK_a value of ascorbic acid is 4.1 in experiment.

Effect of variation of surfactant (Tween 60) concentration

A nonionic surfactant Tween 60 was used in all four systems. It was found that electrical output of the cell increase on increasing the surfactant concentration

Table 1. Effect of variation of dyes concentration in Tween 60 – Dye – Ascorbic acid systems.

System	[Dye] $\times 10^{-5}$	Photopotential (mV)	Photocurrent (µA)
AB	0.3	794.0	295.0
	0.7	902.0	389.0
	1.1	996.0	420.0
	1.5	882.0	381.0
BCP	0.8	720.0	38.0
	1.2	768.0	53.0
	1.6	811.0	65.0
	2.0	763.0	54.0
	2.4	731.0	47.0
Carmine	6.4	816.0	104.0
	6.8	843.0	146.0
	7.2	884.0	190.0
	7.6	851.0	152.0
	8.0	825.0	118.0
BS	4.0	786.0	179.0
	4.4	856.0	194.0
	4.8	919.0	210.0
	5.2	836.0	182.0
	5.6	762.0	168.0

reaching a maximum value. On further increase in concentration of surfactant, a fall in electrical output was observed. The important properties of micellar systems are the ability to solubilize a variety of molecules and substantial catalytic effect on chemical reactions (Fendler and Fendler, 1975). The better electrical output of the photogalvanic cell was observed around the critical micelle concentration of the surfactant. The critical micelle concentration is the concentration of surfactant above which micelles form. The critical micelle concentration of Tween 60 is 0.22. Photoinduced electron transfer processes in micellar systems are potentially important for efficient energy conversion and storage, because surfactants help to achieve the separation of photoproducts by hydrophilic – hydrophobic interaction of the products with the micellar interface (Moroi et al., 1979). Thus, micelles not only solubilized the photosensitizer molecules to a maximum extent around their CMC values but have stabilized also the photogalvanic cell systems.

Effect of variation of photosensitizer concentration

The photogalvanic effect was studied in Amido Black 10B, Bromocresol purple, Carmine, Biebrich scarlet, photosensitizers in presence of Tween 60 and ascorbic acid in photogalvanic cell systems. It was observed that there was an increase in Photopotential (mV), photocurrent (µA) and power (µW) values on increasing the dye concentration (Table 1). A maxima was obtained for a particular value of photosensitizer concentration. On further increase in concentration of a photosensitizer, a decrease in the electrical output was observed. Low electrical output obtained in the lower concentration of photosensitizer due to limited number of photosensitizer molecules to absorb the major portion of the light in the path whereas a higher concentration of photosensitizer does not permit the desired light to reach the molecules near the electrodes and hence, corresponding fall in the electrical output of the cell was obtained.

Absorption properties of dye and dye + Tween 60

All dyes, Amido Black 10B, Bromocresol purple, Carmine and Biebrich scarlet were shown absorption in the visible region and different maximum absorption peak. It is clear from the absorption spectra of different dyes – surfactant combination that the concentration of surfactant shows a remarkable effect on absorbance of dye solution. On initial addition of surfactant solution (from 0.001 to 0.01%) to the dye solution, first a decrease in absorbance was observed. On further increasing the surfactant concentration an enhancement in absorbance was noticed at 0.05% concentration of surfactant (Figure 2a, b, c, d).

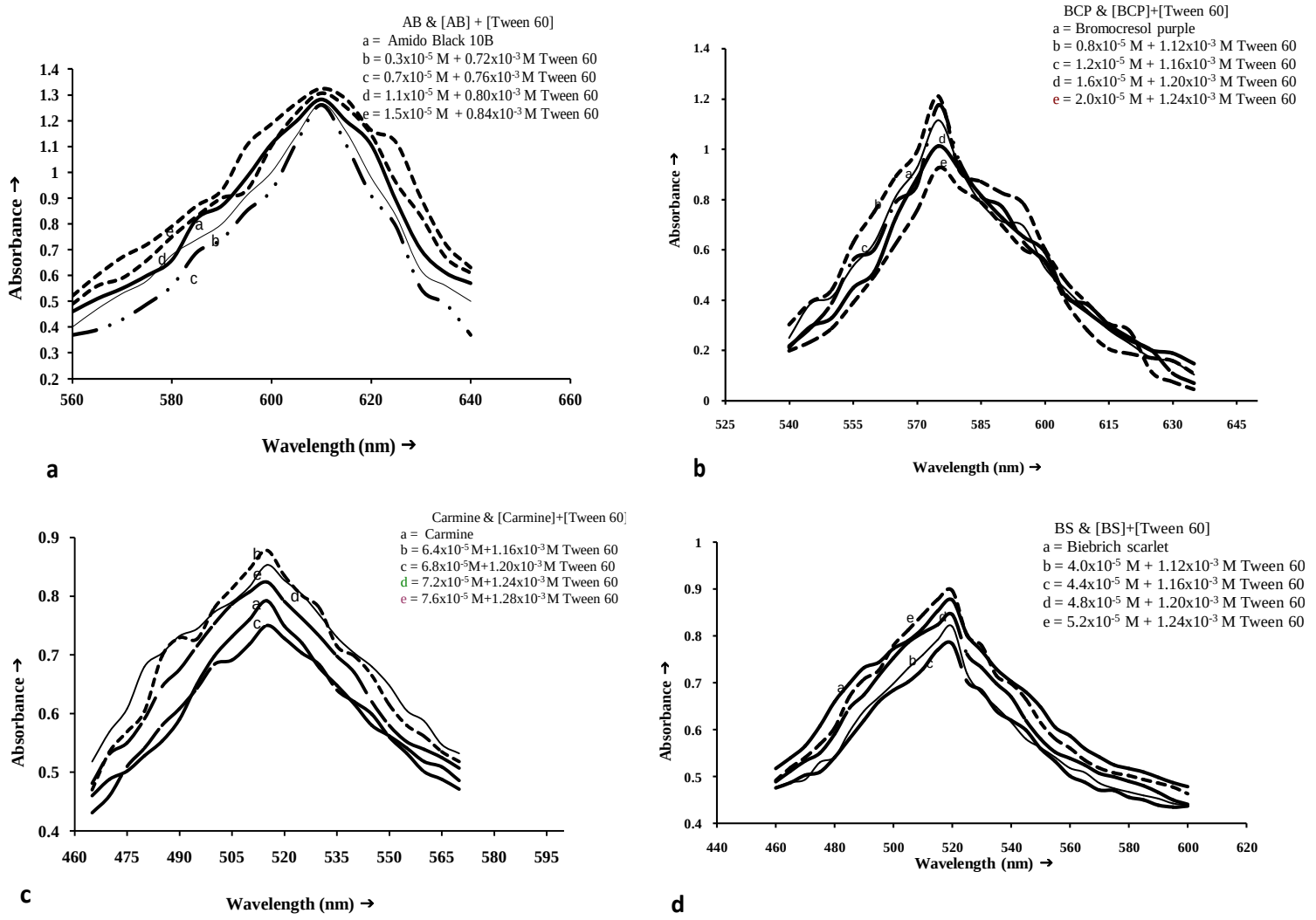

Figure 2. Absorption spectrum of dye and Dye + Surfactant (a) AB and AB- Ascorbic acid; (b) BCP and BCP- Ascorbic acid; (c) Carmine and Carmine- Ascorbic acid; (d) BS and BS- Ascorbic acid.

Effect of diffusion length

Effect of diffusion length on the electrical output (i_{max} and i_{eq}) and rate of initial generation of current ($\mu A\ min^{-1}$) of the photogalvanic cell were observed by using H-cell of different dimensions. The observed results are summarized in Table 2. It was observed that, i_{max} and rate of initial generation of current was found to increase

Table 2. Effect of diffusion length.

Diffusion length (D_L) / Maximum photocurrent i_{max} (µA)	AB system	BCP system	Carmine system	BS system
50	477.0	117.0	198.0	191.0
55	489.0	124.0	228.0	212.0
60	500.0	130.0	250.0	235.0
65	511.0	135.0	281.0	258.0
70	522.0	140.0	308.0	280.0
Rate of initial generation of current (µA min^{-1})				
50	16.44	9.75	8.25	7.95
55	16.86	10.33	9.50	8.83
60	17.24	10.83	10.41	9.79
65	17.62	11.25	11.70	10.75
70	18.00	11.66	12.83	11.66

with diffusion length while i_{eq} shows a negligibly small decreasing behavior. The dye^- and dye are electroactive species in illuminated and dark chambers, respectively. In illuminated chamber dye^- strike at Pt electrode and donate electron to electrode which move through external circuit to reach calomel electrode (in dark chamber), electroactive species dye strike at calomel electrode and accept electron from it then through diffusion, dye^- reach to Pt and dye diffuse to dark chamber. Thus, the electrical output depends on diffusion and conductivity of dye. The conductivity of electro active spices depends on its population between electrodes. As the diffusion length is increased, the volume of photosensitizer solution and intern population of photosensitizer molecules increased leading higher i_{max}. The electro active nature of dye/ dye^- is proved by the fact that i_{max} increase with diffusion length. Therefore, it may be concluded that the main electro active spices are the leuco or semi form of dye^- and the dye in the illuminated and the dark chambers, respectively where as reductant and its oxidation products were act only as electron carries in the path.

Current– potential (i-V) characteristics of the cell

The short circuit current (i_{sc}) and open circuit voltage (V_{oc}) were measured with the help of a digital pH meter (keeping the circuit open) and from a microammeter (keeping the other circuit closed), respectively. The photocurrent and photopotential value in between these two extreme values were recorded with the help of a carbon pot (log 470K) connected in the circuit of the microammeter, through which an external load was applied. The corresponding values of potential with respect to different current values for Tween 60 – dye – Ascorbic acid systems are shown graphically in Figure 3a, b, c, d).

It was observed that the i-V curve deviated from its regular rectangular shapes in all four systems. A point in the i-V curve was determined where the product of current and potential was maximum called power point (pp), and their fill factor values have also been calculated. Some important i-V characteristics of four systems are given in Table 3. On the basis of these comparative data, the order of efficiency of photogalvanic cells on the basis calculated fill factor is: Tween 60 – Bromocresol purple – Ascorbic acid system > Tween 60 – Carmine – Ascorbic acid system > Tween 60 – Biebrich scarlet – Ascorbic acid system > Tween 60 – Amido black 10B – Ascorbic acid system.

Performance (storage capacity) of the cell

The performance or storage capacity of the photogalvanic cells containing four different systems were studied by applying an external load log 470K (necessary to have current at power point) reaches after removing the source of illumination. It was quite interesting observed that the performance of the cell dark was affected appreciably in the presence of various dyes. The performance was determined in terms of $t_{1/2}$, that is, the time required in fall of the power output to its half at power point in dark. Comparative values of power and $t_{1/2}$ of all four systems are given in Table 4 and graphically represented Figure 4.

On this basis of above observations, the order of performance of these cells in dark on the basis of $t_{1/2}$ is as follows: Tween 60 – Carmine – Ascorbic acid system > Tween 60 – Bromocresol purple – Ascorbic acid system > Tween 60 – Amido black 10B – Ascorbic acid system > Tween 60 – Biebrich scarlet – Ascorbic acid system.

Conversion energy efficiency of the cell

Conversion efficiency of all four photogalvanic systems

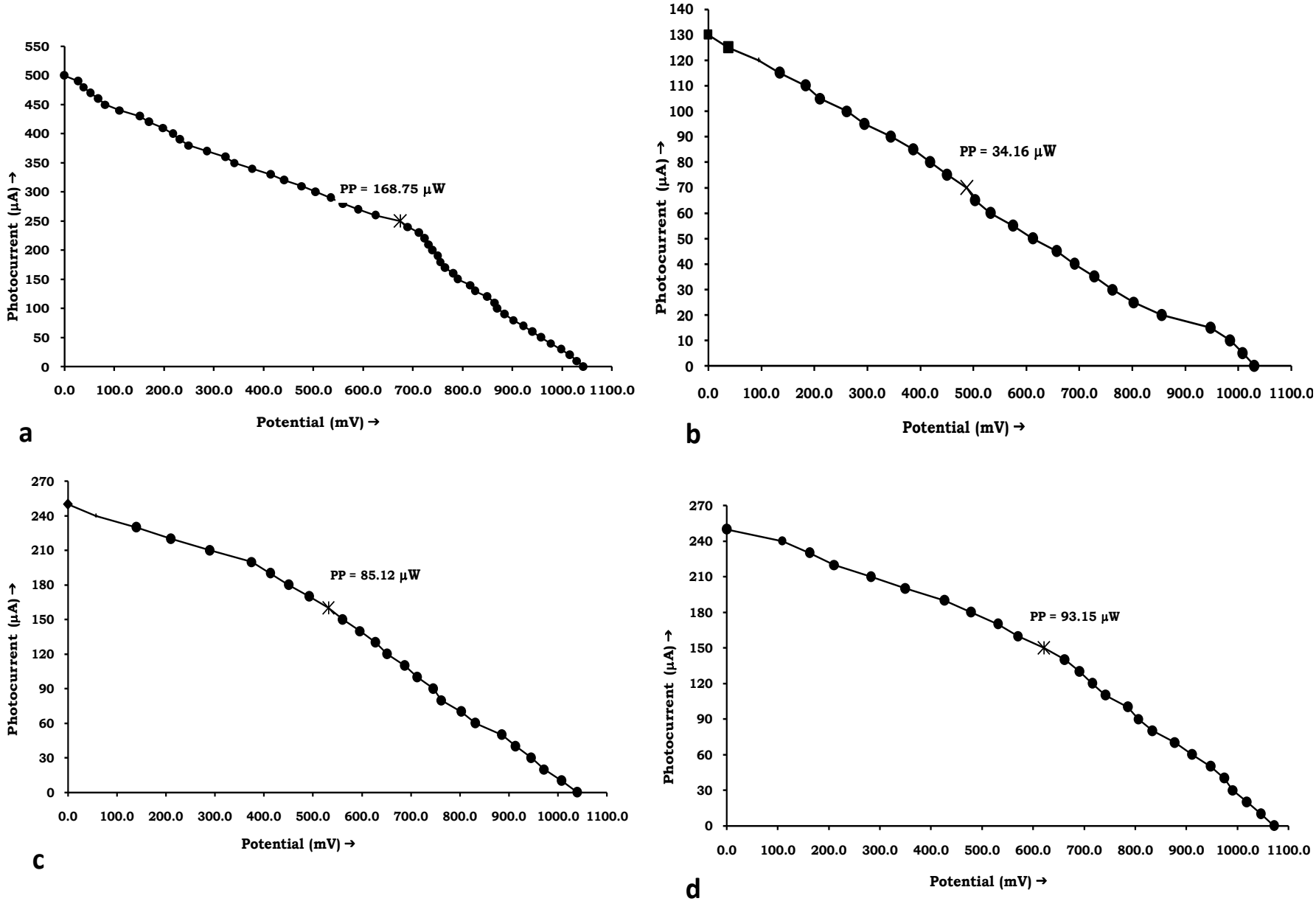

Figure 3. Current – potential (i-V) curve of the cell Surfactant (a) AB- Ascorbic acid; (b) BCP- Ascorbic acid; (c) Carmine- Ascorbic acid; (d) BS- Ascorbic acid system.

Table 3. Current– Potential (i-V) characteristics of the cell.

System	V_{oc} (mV)	i_{sc} (µA)	V_{pp} (mV)	i_{pp} (µA)	Fill factor (*ff*)
Tween 60 – AB – Ascorbic acid	1043	420	675	675	0.38
Tween 60 – BCP – Ascorbic acid	1031	65	488	70	0.50
Tween 60 – Carmine – Ascorbic acid	1040	190	532	160	0.43
Tween 60 – BS – Ascorbic acid	1072	210	621	150	0.41

Table 4. Performance of the photogalvanic cells in dark, conversion energy efficiency and sunlight conversion data.

System	Power (PP) (µW)	$t_{1/2}$ (Min.)	Conversion efficiency η (%)	Sunlight conversion data	
				Potential (mV)	Current (µA)
Tween 60–AB–Ascorbic acid	168.75	130	1.6226	2988	1260
Tween 60–BCP–Ascorbic acid	34.16	150	0.3284	2433	195
Tween 6–Carmine–Ascorbic acid	85.12	170	0.8184	2652	570
Tween 6 –BS–Ascorbic acid	93.15	75	0.8960	2757	630

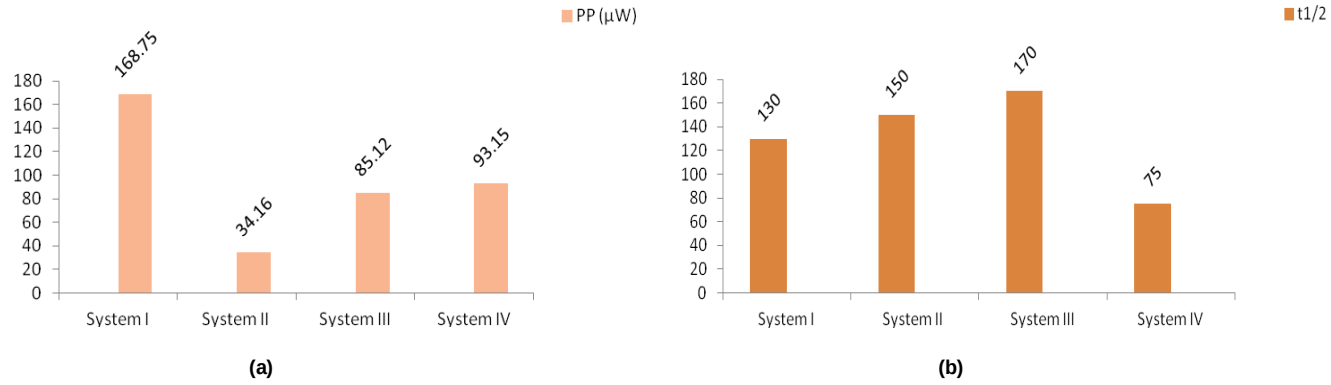

Figure 4. (a) Power and (b) Storage capacities of cell systems.

were calculated with the help of current and potential values at power point (PP) and the incident power of radiations, the conversion efficiency of the cell was determined (Equation 1). The observed values of conversion efficiencies are better than previously reported studies (Gangotri and Gangotri, 2010). The conversion energy efficiency and sunlight conversion data of all four systems are summarized in Table 4 and graphically in Figure 5. On the basis of these observations, photogalvanic cell containing four different dyes systems, the order on the basis of conversion efficiency is: Tween 60 – Amido black 10B – Ascorbic acid system > Tween 60 – Biebrich scarlet – Ascorbic acid system > Tween 60 – Carmine – Ascorbic acid system > Tween 60 – Bromocresol purple – Ascorbic acid system.

$$\text{Conversion efficiency } (\eta) = \frac{V_{pp} \times i_{pp}}{} \times 100\% \quad (1)$$

Mechanism

On the basis of above observations and discussion, the mechanism for generation of electrical output in the photogalvanic cell may be proposed as follow:

Illuminated chamber

On irradiation, dye molecule get excited

$$\text{Dye} \xrightarrow{h\nu} \text{Dye}^* \quad (2)$$

The excited dye molecules accept an electron from reductant and convert into semi or leuco form of dye, and the reductant into its excited state form:

$$\text{Dye}^* + \text{R} \longrightarrow \text{Dye}^-(\text{semi or leuco}) + \text{R}^+ \quad (3)$$

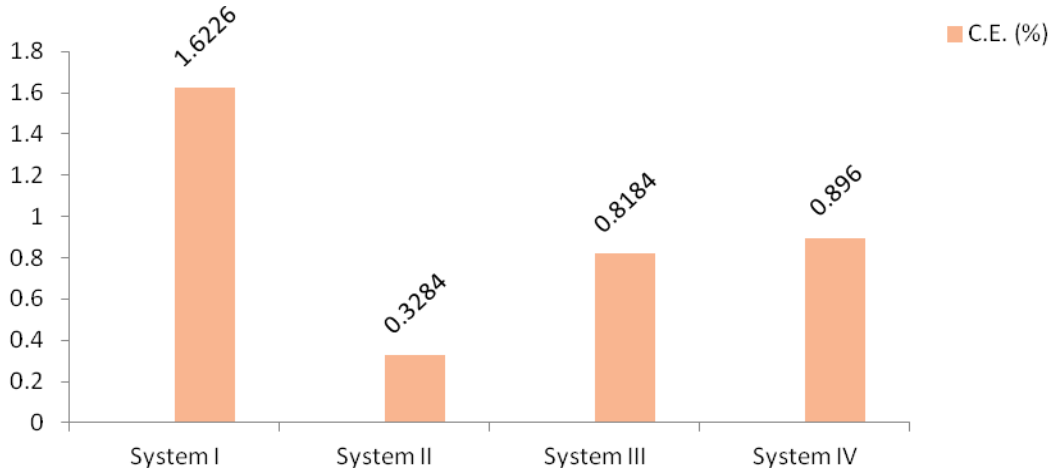

Figure 5. Conversion efficiencies of cell systems.

At platinum electrode: The semi or leuco form of dye loses an electron and converted into original dye molecule.

$$Dye^- \longrightarrow Dye + e^- \quad (4)$$

Dark chamber

At counter electrode

$$Dye + e^- \longrightarrow Dye^- \text{(semi or leuco)} \quad (5)$$

Finally, leuco/semi form of dye and oxidized form of reductant combine to give original dye and reductant molecule and the cycle will go on:

$$Dye^- + R^+ \longrightarrow Dye + R \quad (6)$$

Where, Dye, Dye*, Dye^-, R and R^+ represents the dye, excited form, reduced of dye, reductant and oxidized form of reductant, respectively.

Conclusions

The photogalvanic cells have inbuilt power storage capacity which can be used in absence of sunshine hours (no need of any hardware like batteries). Present work is a successful effort to conversion of solar energy into electrical energy by photogalvanic conversion technology.

Four different dyes (Amido Black 10B, Bromocresol purple, Carmine and Biebrich scarlet) were used as photosensitizers along with a surfactant Tween 60 and Ascorbic acid as a reductant in this work. In all photogalvanic cell systems, possible variations of all parameters are experimentally observed. The fill factor conversion efficiency, power of storage capacity of all systems was determined. On the basis of these results, conversion efficiency point of view Tween 60 – Amido black 10B – Ascorbic acid system is a most efficient followed by Tween 60 – Biebrich scarlet – Ascorbic acid system, Tween 60 – Carmine – Ascorbic acid system and Tween 60 – Bromocresol purple – Ascorbic acid system. Storage capacity point of view Tween 60 – Carmine – Ascorbic acid system is a most efficient followed by Tween 60 – Bromocresol purple – Ascorbic acid system, Tween 60 – Amido black 10B – Ascorbic acid system and Tween 60 – Biebrich scarlet – Ascorbic acid system.

Finally, it may be concluded that Amido black 10B and Carmine dyes are efficient to be used in photogalvanic cell for conversion efficiency and storage capacity and in view of generation of electrical out-put. In future, efforts will be made to enhance these two factors along with their practical/field implementation.

ACKNOWLEDGEMENTS

Authors are thankful to UGC New Delhi for providing financial assistance under UGC major research project [40 – 55/ 2011 (SR)].

Nomenclature: $\mathbf{V_{oc}}$**,** Open circuit voltage; Δ**V,** photopotential; $\mathbf{i_{max}}$**,** maximum photocurrent; $\mathbf{i_{eq}}$**,** equilibrium photocurrent; $\mathbf{i_{sc}}$**,** short circuit current; $\mathbf{i_{pp}}$**,** current at power point; $\mathbf{V_{pp}}$**,** potential at power point; ***f f*****,** fill factor; **η,** conversion efficiency; $\mathbf{D_L}$**,** diffusion length; **A,** electrode area; **PS,** photosensitizer; **AB,** amido black 10B; **BCP,** bromocresol purple; **BS,** biebrich scarlet.

REFERENCES

Albery WJ, Archer MD (1977). Optimum efficiency of photogalvanic

cells for solar energy conversion. Nature 270:399-402.
Ameta SC, Punjabi PB, Vardia J, Madhwani S, Choudhary S (2006). Use of bromophenol red-EDTA system for generation of electricity in photogalvanic cell. J. Power Source 159:747-751.
Armstrong S, Hurley WG (2010). A new methodology to optimize solar energy extraction under cloudy conditions. Renew. Energy 35:780-787.
Balzani V, Credi A, Venturi M (2008). Photochemical conversion of solar energy. Chem. Sus. Chem. 1:26-58.
Bisquert J, Belmonte GG (2002). Importance's analysis of glvano statically synthesized polypyrrole films, correlation of ionic difference and capacitance parameters with the electrode morphology. Electrochim. Acta. 47:4263-4272.
Fendler EJ, Fendler JH (1975). Advanced Physical Chemistry, Academic Press, London. P. 8.
Folcher G, Paris J (1983). Photogalvanic cell. J. US Patent. 439:1881.
Gangotri KM, Gangotri P (2010). Studies of the miceller effect on photogalvanics: EDTA-Sarfanine O- DSS system. Int. J. Energy Res. 34:1155-1163.
Gangotri KM, Indora V (2010). Studies in photogalvanic effect in mixed reductant system for solar energy conversion and storage:Dextrose-Ethylenediaminetetraacetic acid-Azur A system. Solar Energy. 84:271-276.
Genwa
KR, Kumar A (2012). Role of acridine orange-sodium lauryl sulphate system in photogalvanic cell for solar energy conversion. Int. J. Renew. Energy Technol. 3 174-188.
Jana AK (2000). Solar cells based on dyes. J. Photochem. Photobiol. A. Chem. 132:1-1.
Kaneko M, Yamada A (1977). Photopotential and photocurrent induced by tolusafranine ethylenediaminetetraacetic acid system. J. Phys. Chem. 81:1213-1215.
Memming R (1980). Solar energy conversion by photoelectrochemical processes. Electrochim. Acta. 25:77-88.
Meyer GJ (2005). Molecular approaches to solar energy conversion with coordination compounds anchored to semiconductor surfaces. Inorg. Chem. 44:6852-6864.
Moroi Y, Infelte PP, Gratzel M (1979). Light initiated redox reaction in functional micellar assemblies. J. Am. Chem. Soc. 101:573-579.
Murthy ASN, Reddy KS (1979). Photochemical energy conversion studies in system containing methylene blue. Int. J. Energy Res. 3:205-210.
Naman SA, Karim ASR (1984). Efficiency of photogalvanic cells with various dyes. J. Solar Energy Res. 2:31- 41.
Pan RLR, Bhardwaj R, Gross EL (1983). Photochemical energy conversion by a thiazine photosynthetic photoelectrochemical cell. J. Chem. Technol. Biotech. Chemtech. 33:39-48.
Rabinowitch E (1940a). The photogalvanic effect I: the photochemical properties of the thionine-iron system. J. Chem. Phys. 8:551-559.
Rabinowitch E (1940b). The photogalvanic effect II: the photogalvanic properties of thionine-iron system. J. Chem. Phys. 8:560-566.
Ratcliff EL, Zacher B, Armstrong NR (2011). Selective interlayer's and contacts in organic photogalvanic cells J. Phys. Chem. Lett. 2:1337-1350.
Rideal EK, Williams EG (1925). The action of light on the ferrous iodine iodide equilibrium. J. Chem. Soc. Trans. 127:258-269.
Sharma U, Koli P, Gangotri KM (2012). Solar energy conversion and storage: rodamine B – fructose photogalvanic cell. Renew. Energy. 37:250-258.
Yadav S, Lal C (2010). Photogalvanic cell as a device for solar energy conversion and storage: EDTA-New methylene blue and safranine O system, Energy Sources Part A. Energy Sources Part A. 32:1028-1039.

academicJournals

Vol. 8(29), pp. 1526-1536, 9 August, 2013
DOI: 10.5897/IJPS2013.3957
ISSN 1992 - 1950 © 2013 Academic Journals
http://www.academicjournals.org/IJPS

International Journal of Physical Sciences

Full Length Research Paper

Role of finite element method (FEM) in predicting transverse modulus of fiber-reinforced polymer (FRP) composites: A revelation

Srihari P. Anne[1]*, Ramana K. V.[1], Balakrishna Murthy V.[2] and Rao G. S.[2]

[1]Department of Mechanical Engineering, K L University, Vaddeswaram, Guntur District, India.
[2]Department of Mechanical Engineering, V R Siddhartha Engineering College, Vijayawada, India.

Accepted 29 July, 2013

The present investigation aims to validate finite element method (FEM) in micromechanical analysis of a unidirectional continuous fiber reinforced composites and experimental verification of results in case of fiber-matrix debond. Available analytical models are reviewed, compared and are seldom in agreement with each other in case of transverse modulus of unidirectional continuous fiber reinforced composites. Reasons for variation of these models are analyzed and their limitations are discussed. FEM of a square representative volume element (RVE) are developed to simulate various conditions such as matrix/fiber dominated cases (in volume and stiffness) and fiber-matrix interface debond in ANSYS v12 to facilitate comparison with the available analytical results. Numerical results are compared with the approximate as well as exact analytical models and are found to be in very close agreement with exact analytical results. To simulate fiber reinforced composite behavior close to a mathematical model of square RVE, a specimen with a combination of two metals is designed, fabricated and tested to determine the transverse modulus. FEM of a regular square RVE is modified to suit the specimen conditions such as finite dimensions relative to fiber and possible fiber-matrix interface debond. FEM results are found to be in good agreement with the experimental results and thus the validity and applicability of FEM in predicting transverse modulus of fiber reinforced composites is established.

Key words: Fiber-reinforced polymer (FRP) composites, micromechanics, transverse Young's modulus, fiber-matrix debond.

INTRODUCTION

The inherent anisotropy of composites makes it compulsive to test the components case by case based on the loading pattern and application. In this process, experimental methods not only demand higher levels of skills right from fabrication to testing of the specimen but also are time taking. Alternative empirical, semi-empirical, approximate and exact analytical models that are available in micromechanical analysis to determine the mechanical properties of composites are based on certain assumptions, for mathematical simplification, offer satisfactory results in some cases but do not cover the entire spectrum of material compositions. On the other hand, finite element method (FEM) that can cater to varying requirements in analyses is a convenient tool for providing quicker and economical solutions but needs validation by other means. The present study is a step made towards benchmarking FE, analytical and experimental analyses in case of transverse Young's modulus.

A large number of analytical models with varying

*Corresponding author. E-mail: srihari.anne@kluniversity.in.

degrees of accuracy are available for predicting the mechanical properties of unidirectional composites. They range from the simple rule of mixtures (ROM) to methods based upon the use of elastic energy principles. In general, they incorporate certain simplifications of the physical state of materials that resulted in theories which do not satisfactorily correlate with the experimental data. Unlike ROM that works perfectly for predicting longitudinal Young's modulus, the inverse ROM (IROM) fails to give satisfactory results for transverse Young's modulus (referred as transverse modulus in this paper) in all cases. This may be one of the reasons why researchers worked on developing several models for predicting the transverse modulus. Modified inverse IROM (MIROM) has taken into account the lateral contraction of matrix material under tension due to Poisson's effect and accommodated it accordingly (Isaac and Ori, 1994; Robert, 1999; Autar, 1997). It is demonstrated that a combination of ROM and IROM can be adapted to suit theoretical modeling of a composite material by considering a combination of parallel and series orientation of rectangular elements of fibers scattered over entire area of representative volume element (RVE) and proposed two models: a horizontal and a vertical models to predict transverse modulus (Jacquet et al., 2000). Halpin-Tsai and Kardos (1976) have developed a semi-empirical equation to determine the transverse modulus by taking the shape of the fiber cross section into consideration as reinforcing efficiency factor. Neilson (1970) modified the Halpin-Tsai equation by introducing a packing factor (ϕ_{max}) for square, hexagonal and random fiber packing arrays. Hirsch (1962) model is a combination of both ROM and IROM. When the value of x = 0, the relation reduces to IROM and when x = 1, it reduces to ROM. The value of x depends on the fiber orientation with respect to the direction of loading. Kalaprasad et al. (1997) mentioned Neilson and Hirsch models in their paper and compared the available experimental data with various analytical models for short sisal-LDPE composites. Alfredo (2000) derived a closed form of expression based on simple mechanics of a repeating square cell for predicting transverse modulus. Hui-Zu and Tsu-Wei (1995) have used elasticity theory and derived expressions for exact transverse modulus of a square RVE. Also, they have extended the theory to find a solution for the case of fiber matrix debonding by using an elastic contact model. Mistou et al. (2000) made a comparative study of elastic properties of composite materials by quasi-static as well as ultrasonic methods. It is observed that the ultrasonic method of testing is efficient, accurate and easy to conduct in comparison with tests on UTM. Stagni (2001) derived a formula for evaluating the effective transverse modulus of multilayered hollow fiber composites. The author observed that under certain conditions, increase in porosity results in increased transverse modulus. Muhannad et al. (2011) compared experimental results of longitudinal and transverse moduli with the values from four micromechanical models of a unidirectional fiber-reinforced polymer (FRP) composite (E-Glass/Epoxy) of 37% volume fraction. However, none of the analytical results matched mutually and also with the experimental results. The reason behind analytical models not concurring with each other are obvious but the experimental results not agreeing with any one of the analytical results could be due to random arrangement of fibers. Li and Wisnom (1994) reviewed typical finite element formulations and models for unidirectional composite materials and shown that finite element analysis (FEA) provides more accurate and detailed characterization of composite properties for complicated geometries and constituent property variations. Theocaris et al. (1997) proposed a simple numerical homogenization method to predict effective transverse elastic modulus of fiber reinforced composites and the results are compared with existing analytical models. The authors observed that the results of homogenization are close to the results of mesophase concept and have only limited correlation with Hashin-Rosen model. Haktan and Dilek (2007) made a study of effective thermal expansion coefficients of composite materials by micromechanical FE modeling in ANSYS. The results are compared with other analytical and experimental data. While the results of all models are in close agreement with each other in case of α_1, they differed well in case of α_2 except that FEA results matched with some of the experimental results. The mismatch could be due to randomness of fibers in matrix. Bhaskar and Mohammed (2012) used FEA to study transverse modulus along with other mechanical properties of fiber reinforced composites. The numerical results are compared with analytical solutions of IROM and Halpin-Tsai and their FEA results are not in close agreement with Halpin-Tsai's for all volume fractions at E_f/E_m around 4. However, the authors have not validated the results by any other means.

From this literature survey, it is apparent that available analytical models and FEA results are matching only in few cases and no evidence is available regarding validation of FEA results with exact analytical results. Also, the information about the basis for comparing analytical and FE models supported by subsequent validation is not available in the literature so far referred. The investigation regarding fiber arrangement in the test specimen as per RVE modeled in FEA seems to have been unexplored. In the present work, test specimens are specifically designed and fabricated to match the RVE modeled in FEA and transverse moduli results from experimental and FEA are compared with exact and other analytical models for mutual validation.

REVIEW OF ANALYTICAL MODELS

Of the available analytical models, popular models are

considered for comparison and presented here for convenience.

The IROM

The classical ROM predicts the longitudinal Young's modulus (E_1) of a composite material accurately but the IROM (Isaac and Ori, 1994; Robert, 1999; Autar, 1997) fails to predict transverse modulus (E_2) in general and particularly at higher fiber volume fractions. The IROM fails in the case of voids as well. Equation (1) works perfectly for those slab models (with negligible Poisson's effect) that are placed in series which is not the case with fiber reinforced composites in reality and hence the inevitable failure.

$$E_2 = \frac{E_f.E_m}{E_f.V_m + E_m.V_f} \quad (1)$$

Modified IROM (MIROM)

Modifications to IROM are suggested by various researchers based on specific assumptions. The MIROM as suggested by Ekvall (Isaac and Ori, 1994; Robert, 1999; Autar, 1997) and given as Equation (2) considers the Poisson's effect of matrix and the relation does not attempt to take care of the actual geometry of the composite. Even then the equation fails in fiber dominated and fiber like void cases.

$$E_2 = \frac{E_f.E'_m}{V_f.E'_m + V_m.E_f(1-\nu_m^2)} \quad \text{where} \quad E'_m = \frac{E_m}{(1-2\nu_m^2)} \quad (2)$$

Jacquet's horizontal and vertical models (JA-H and JA-V)

Jacquet et al. (2000) made an attempt to assess the transverse modulus of a unidirectional composite by using two novel models (horizontal and vertical) based on classical ROM. The horizontal (JA-H) and vertical (JA-V) models are given as Equations (3a) and (3b).

$$\frac{1}{E_2} = \frac{\sqrt{V_f}}{E_f\sqrt{V_f} + E_m(1-\sqrt{V_f})} + \frac{1-\sqrt{V_f}}{E_m} \quad (3a)$$

$$E_2 = \frac{E_f.E_m}{E_m + E_f(1-\sqrt{V_f})/\sqrt{V_f}} + (1-\sqrt{V_f})E_m \quad (3b)$$

Though the treatment is simple, the assumption such as decomposing of fiber of any shape into small rectangular elements that are scattered in matrix in a regular array is unrealistic and correct results can never be expected from such models.

Halpin-Tsai model (H-TSAI)

The semi-empirical relation for transverse modulus suggested by Halpin –Tsai (1976) is given as Equation (4)

$$E_2 = E_m\frac{(1+\xi.\eta.V_f)}{(1-\eta.V_f)} \quad \text{where} \quad \eta = \frac{E_f - E_m}{E_f + \xi.E_m} \quad (4)$$

and ξ is reinforcing efficiency factor for transverse loading that depends on the fiber cross section and the kind of packing geometry. The value of ξ is suggested as lying between 1 and 2 by several authors (Muhannad et al., 2011; Li and Wisnom, 1994; Theocaris et al., 1997) for prediction of E_T. The selection of ξ value on empirical basis limits the usage of this equation for a generalized case.

Modified Halpin-Tsai model (MH-TSAI)

Neilson (1970) modified the Halpin-Tsai equation by including the maximum packaging fraction ϕ_{max} of the reinforcement and the equation transformed to

$$E_2 = E_m\frac{(1+\xi.\eta.V_f)}{(1-\eta.\phi_{\max}.V_f)} \quad (5)$$

where $\phi_{\max}$ is packing factor and is given as 0.785 for square array, 0.907 for hexagonal array and 0.82 for randomly oriented. Though this relation is clear about fiber packing factor, the empirical value of ξ still limits its application for a generalized case.

Hirsch model

Hirsch (1962) model is a combination of parallel and series models and the transverse modulus is calculated according to Equation (6).

$$E_2 = x\,(E_mV_m + E_fV_f) + (1-x)\frac{E_fE_m}{E_mV_f + E_fV_m} \quad (6)$$

As can be seen from the structure of the equation, this model is a combination of ROM and IROM, and the value of x depends on the fiber orientation with respect to loading direction. For transverse modulus where the angle between fiber and loading directions is 90°, x becomes zero and hence this model reduces to IROM.

Morais model

Morais (Alfredo, 2000) derived a closed-form micromechanical expression for predicting the transverse modulus of a square RVE. He claims that his results

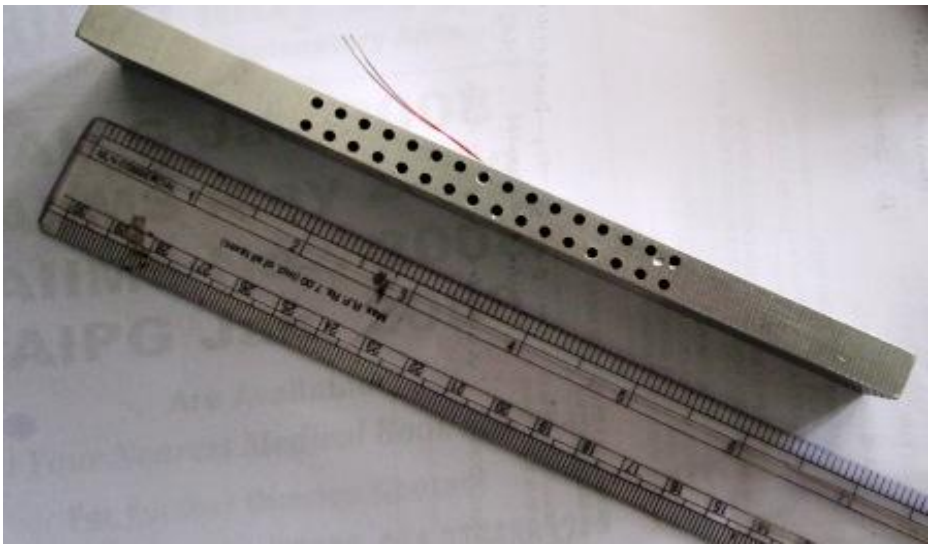

Figure 1. Specimen with holes drilled across thickness.

match with 3-D FE result of a hexagonal unit cell. It is observed that Morais' expression is a modification of Jacquet's vertical model by introducing Poisson's effect of matrix into the relation.

$$E_2 = \frac{\sqrt{V_f}}{\frac{\sqrt{V_f}}{E_f} + \frac{(1-\sqrt{V_f})(1-\nu_m^2)}{E_m}} + (1-\sqrt{V_f})\frac{E_m}{(1-\nu_m^2)} \quad (7)$$

Hui-Zu and Tsu-Wei (1995) developed an elastic constant model to predict transverse modulus, Poisson's ratio and shear modulus of unidirectional fiber composites with interfacial debond. The elastic deformation formula of the fiber under contact pressure is derived by using elasticity theory. Results are presented for two limiting cases of perfect bonding and fiber like void.

In exact analytical approach, the whole body is considered as one entity and the equilibrium equations of one infinitely small element within the body are integrated to the boundaries to get an exact solution. However, in cases where integration is not possible due to mathematical limitations such as physical discreteness, the solution is not possible always. Apart from the geometric limitations of the material body, there are other issues such as material discontinuity, complex material combinations and loading pattern etc., which are difficult to idealize and the accuracy of the solution ultimately depends on the order of the equation making the analytical methods more and more case sensitive.

EXPERIMENTAL INVESTIGATION

Preparation of test specimen

Analytical methods used for determining mechanical properties of composite materials require a reference for their validity and obviously experimental results provide the answer. Test specimens prepared invariably differ from theoretical models in many ways and there is bound to be disagreement between experimental results and analytical outcome. Fabrication of composites with conventional fibers and matrices close to the mathematical model is relatively difficult due to minute fiber diameter and since it is only for validation of methodology, metals are chosen as constituent materials for the present study. The isotropic nature of metals and the ease with which a given geometrical accuracy can be achieved on metals are reasons for choosing different metals to prepare a metal composite for the present study. The aim is to make a test specimen close to the mathematical model with a purpose to establish a verifiable relation between theory and practice. Aluminum, copper and mild steel are chosen for preparing the composite specimens with aluminum as matrix and the rest as fibers.

Three categories of composite specimens are prepared viz., copper-aluminum, mild steel-aluminum, and voids-aluminum (fiber like voids). Aluminum flats of 175*25*10 mm dimensions are taken as specimen blanks. While maintaining the length and width of the specimen as per ASTM D 3039/D3039M-08 (2008), the thickness of the specimen is taken as per the machining requirements. 2 mm diameter holes are drilled across 10 mm thick faces (along 25 mm width) as shown in Figure 1. Drilling is done on an NC machine taking sufficient care to maintain spacing between the holes. Each sample accommodated 32 holes (16 in each row) and the spacing of holes is according to the machining limitations. The fiber volume fraction achieved by this arrangement is 12.566%. An initial attempt to drill 1 mm diameter holes to achieve higher fiber volume fraction resulted in breaking of too many drill bits even on numerically controlled machine and hence the decision to go for higher diameter. Before going for 2 mm diameter holes, it is ensured that 2 mm diameter copper and mild steel wires are available commercially.

Twenty-five millimeter long pieces are cut from copper and mild steel wire rolls in sufficient numbers. Wires are driven into the holes by gentle tapping with a nylon mallet. Moderate force was needed to drive each fiber piece into a hole that is an indication of generous contact between the male and female surfaces. This ensured sufficient gripping due to the interference fit of the assembly between fibers and matrix without any mechanical bonding. For each category of the composite three specimens are prepared bringing the total number of specimens to nine. These specimens

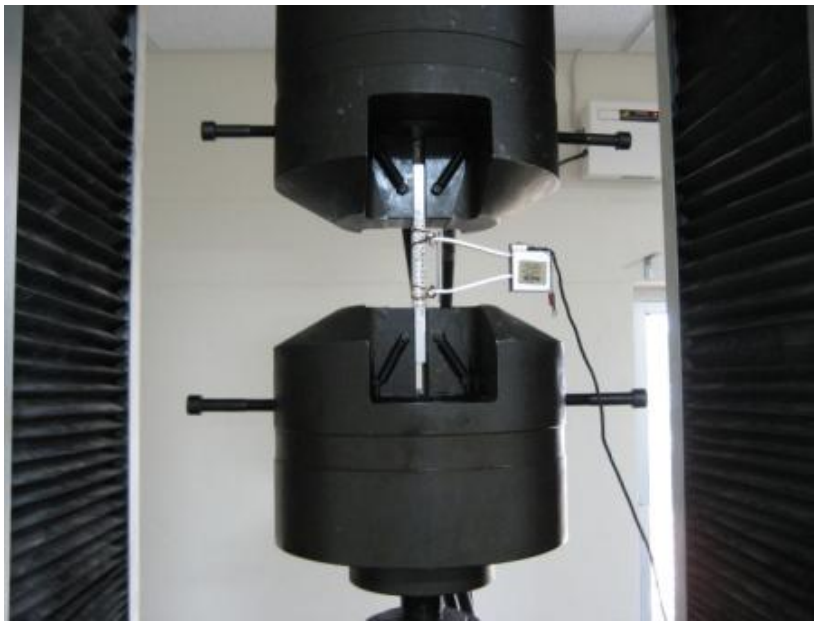

Figure 2. Test set-up on UTM.

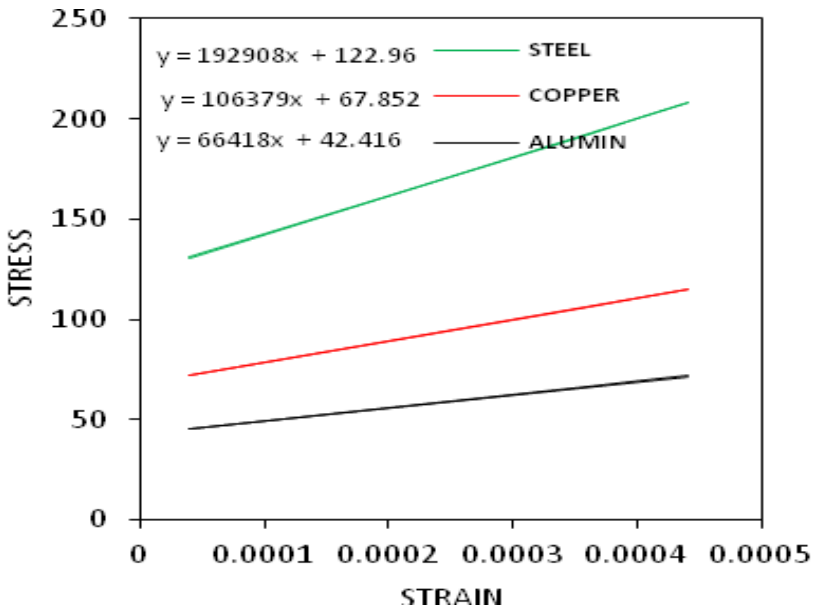

Figure 3. Stress-strain plot for one set of constituent materials.

are tension tested on a micro-computer controlled electronic UTM of 400 kN capacity as shown in Figure 2 at a cross head speed of 1 mm/min. An electronic extensometer of 1 µm least count is used to measure the extension and the test data is recorded automatically.

Determination of Young's modulus of constituent materials

Though, Young's modulus of constituent materials could be taken from the standard data, it is opined that the values once again be experimentally determined for closeness and subsequent substitution in analytical and FE models since the aim of the present study is validation. 175*25*10 mm aluminum blanks are tested on UTM and for copper and steel wires, three point bending tests are conducted on a 2-ton electronic tensometer (model: METM 2000 ER-I). For each material, three samples are tested and the value of E is calculated from the slope of linear portion of stress-strain plot obtained. The test data is tabulated in Table 1. Figure 3 shows one set of stress-strain plots for three types of specimens with corresponding trend line equations indicated along.

Table 1. Results of constituent materials tested for longitudinal Young's modulus.

Specimen description	TEST 1 E_1 (GPa)	TEST 2 E_1 (GPa)	TEST 3 E_1 (GPa)	Average value
Aluminum blank	67.501	65.521	66.418	66.48
Copper wire	106.379	105.199	107.624	106.40
Mild steel wire	195.966	191.416	192.908	193.43

Table 2. Results of composite specimens tested for transverse modulus.

Composite material description	Test 1 GPa	Test 2 GPa	Test 3 GPa	Average E_2
Mild steel-aluminum	51.668	51.364	51.429	51.487
Copper-aluminum	51.036	51.109	51.261	51.135
Void like fiber-aluminum	49.469	49.223	49.545	49.412

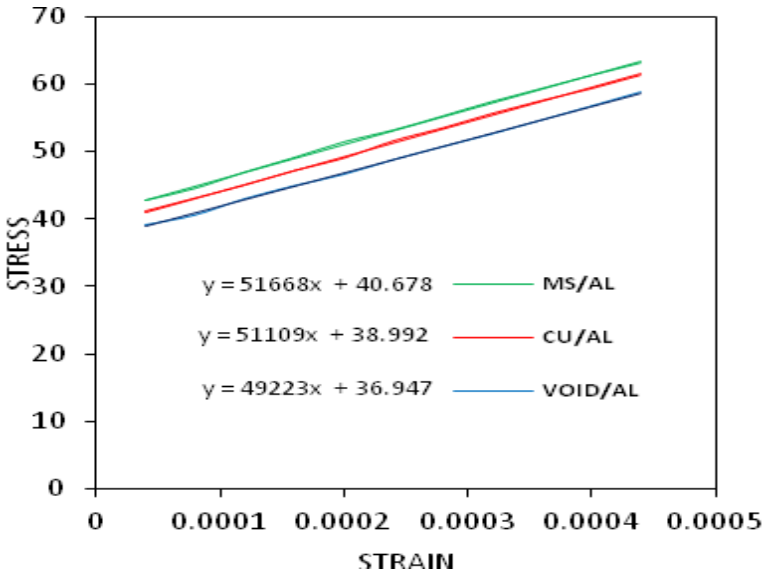

Figure 4. Stress-strain plots for one set of composite material.

Determination of transverse modulus of composite specimens

Three samples for each category of composites are tested and the values of transverse moduli (E_2) are calculated from the slope of the linear portion of stress-strain plots obtained from the recorded data. The test results are tabulated in Table 2. Figure 4 shows one such set of plots with corresponding trend line equations.

Numerical approach

In numerical approach, though approximate, the theme of treatment is same at local as well as global levels. Decomposing any shape and effectively encompassing the complete material geometry through finite number of fundamental elements is the basic principle behind the numerical method. Formation of local governing equations in terms of geometry, material property and loading pattern while simultaneously maintaining local-global connectivity, numerical approach will always come up with a solution. However, validation of this solution requires bench marking that forms the basis of the present work. Numerical errors are reduced by proper choice of the element and its size and the accuracy of the outcome can be checked by testing for convergence.

An RVE in the form of a square unit cell in cross-section is adapted for analysis and a one eighth unit cell (one-fourth in cross-section and half in longitudinal direction) is modeled by taking the advantage of symmetry. The geometry of FE model and the composite's constituent properties are so selected to cover sufficiently a large range of fiber volume fractions (V_f = 0.1 to 0.72) and material combinations (E_f/E_m = 100:1 to 1:100) in order to compare FE results with available analytical results. The dimensions of the cell are 250*250*10 mm and fiber radius is calculated as per the required volume fraction using the relation $r = \sqrt{4*V_f*250*250/\pi}$. For convenience of analysis, scaling up of cell size is done without loss of proportionality. Processing of the required steps in FEM such as generation of element matrices, assembling of system equations and solving them under prescribed constraints for nodal deformations of any structural problem is a built in feature of ANSYS software, provided the problem is clearly

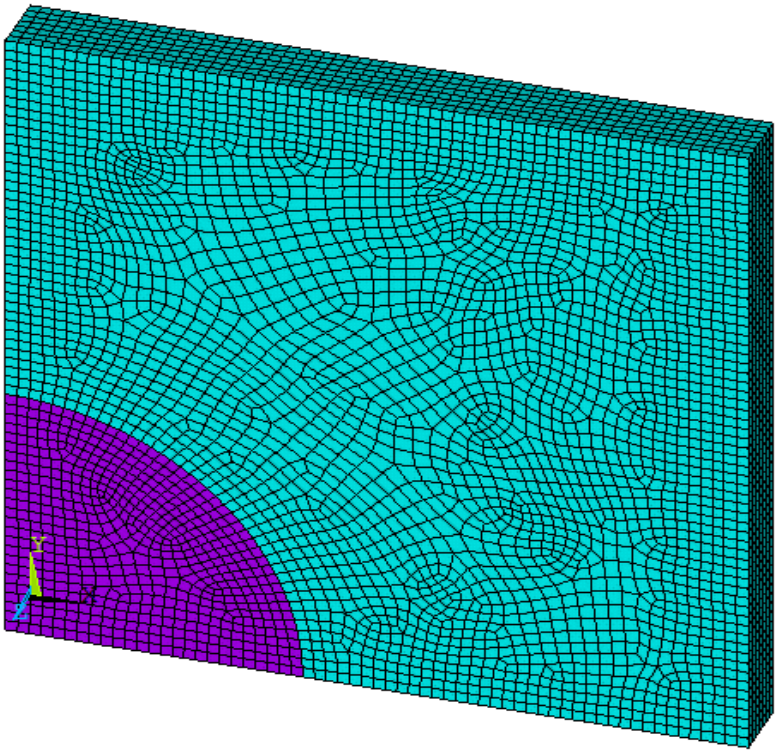

Figure 5. FE model showing mesh with element edge length 4.

defined and discretization is made to the satisfaction of results, which is a proven tool universally used by many researchers for the analysis of composite materials. Hence, the present problem is modeled in ANSYS straight away without resorting to any other programming routines. SOLID 20 NODE 95 element of ANSYS is used to create FE mesh which is a quadratic brick element that is best suited for curved boundaries. Mesh refinements are made with different element edge lengths and convergence is verified at maximum mismatch conditions (E_f/E_m = 100:1 and V_f = 0.72). It is observed that at element edge lengths 4 and below the results have converged for this model. FE model with an element edge length 4 is shown in Figure 5.

Symmetric boundary conditions are applied on negative faces of the Cartesian coordinate system which can be observed in Figure 5. Multipoint constraints are imposed on the boundary planes x, y and z to ensure uniform strain in respective directions. A uniform tensile load of 1 MPa is applied on the x-face to observe a uni-axial state of stress that facilitates usage of simple Hooke's law for calculating Young's modulus, while the fibers are parallel to z-axis. A similar model as above, with appropriate changes for fiber-matrix debond case, is developed. Boundary conditions and loading are kept without any change. This model is necessitated as the fibers in the specimen are not bonded to the matrix by any means.

RESULTS AND DISCUSSION

Comparison of analytical and FE models in fiber dominated cases

Variation of normalized transverse modulus (E_2/E_m) with respect to V_f for E_f to E_m ratios of 100:1, 50:1, 21.19:1 and 5.5:1 (Hui and Tsu-Wei, 1995) are shown in Figures 6 to 9. It is observed that, in Figures 6 and 7, the analytical models predict lower values of E_2 with increasing V_f in comparison to FE model. IROM model predicts the least value for E_2, while FE model predicts the highest and the rest of the models are positioned in between. It is also observed that the differences in values of E_2 between each of these models and FE model is progressively increasing with increasing V_f. As mentioned earlier, IROM works with assumption of slab models where fiber and matrix are assumed to be placed in series, which is why this model predicts least values and obviously fails to give accurate results. Though Poisson's effect of matrix is considered in MIROM, the basic assumption of IROM remains within and hence the results are marginally improved in this case. JA-H and JA-V models (Jacquet et al., 2000) decompose fibers of any shape into minute sqare or rectangular blocks to overcome the deficiencies of IROM that resulted in mariginal improvement. However, these results are still below FEM values.

Halpin-Tsai model (Halpin-Tsai and Kardos, 1976) has an empirical term ξ introduced into the relation whose value depends on the fibers' cross sectional shape, fiber volume fraction and fiber packing. It is suggested in the literature that the value of ξ be found from experiments for a given set of known constituents of a composite which varies from 1 to 2. The values of E_2 for

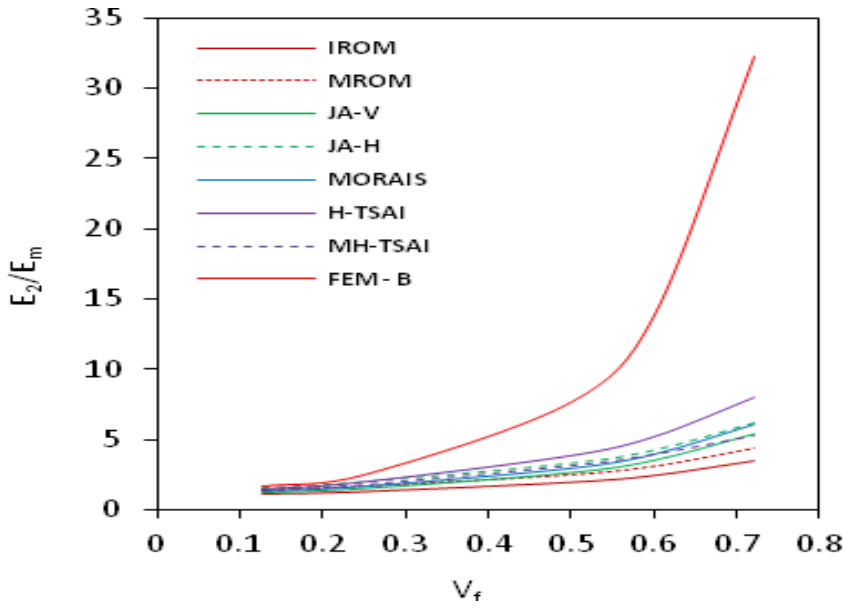

Figure 6. Variation of normalized E_2 with V_f (for E_f/E_m = 100:1).

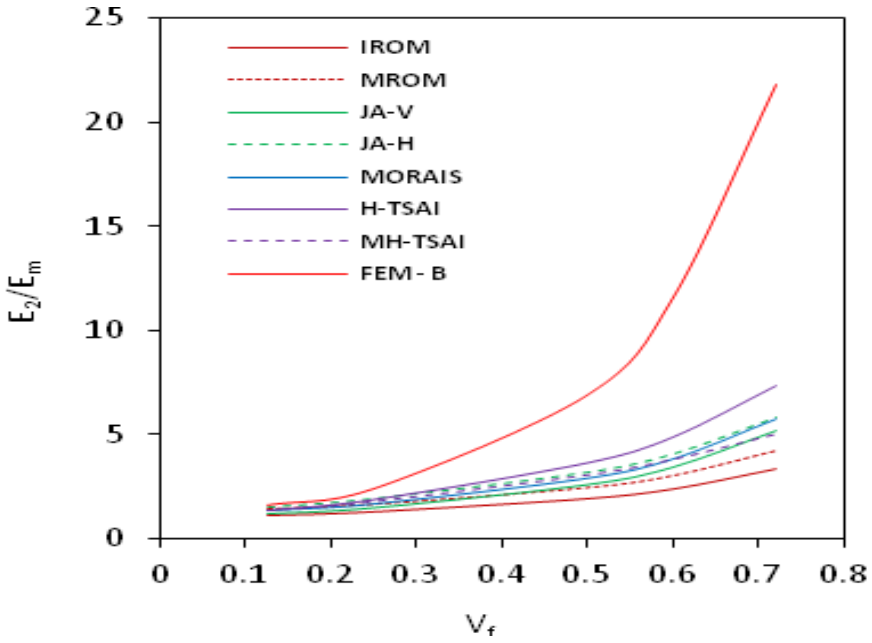

Figure 7. Variation of normalized E_2 with V_f (for E_f/E_m = 50:1).

Halpin-Tsai model in the present study are calculated by taking ξ=2 as suggested in the literature for circular fibers. It is observed that Halpin-Tsai predicts higher values than all other analytical models considered so far here. Since the value of ξ provided here is not for a particular case, these values cannot be treated as exact for any general case. MH-Tsai (Neilson, 1970) relation takes care of the fiber packing due to the term ϕ but the V_f still has no role in it and hence the values of E_2 obtained cannot be accurate at all volume fractions. Morais' model (Alfredo, 2000) which appears to be in line with JA-V equation by considering the Poisson's effect of matrix has shown further improvement, but the assumptions regarding decomposition of fibers that form the basis of JA-V makes this model still unrealistic. It is also observed that the magnitude of E_2 has not been

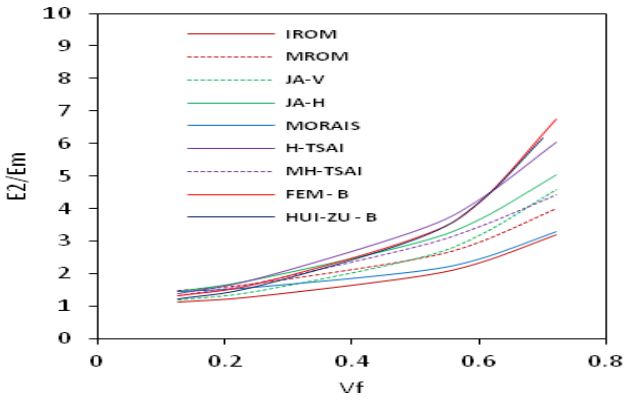

Figure 8. Variation of normalized E_2 with V_f (for E_f /E_m = 21.19:1, bonded).

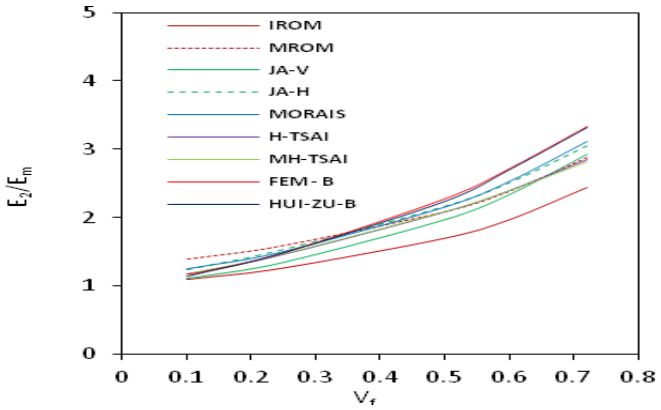

Figure 9. Variation of normalized E_2 with V_f (for E_f /E_m = 5.5:1, bonded).

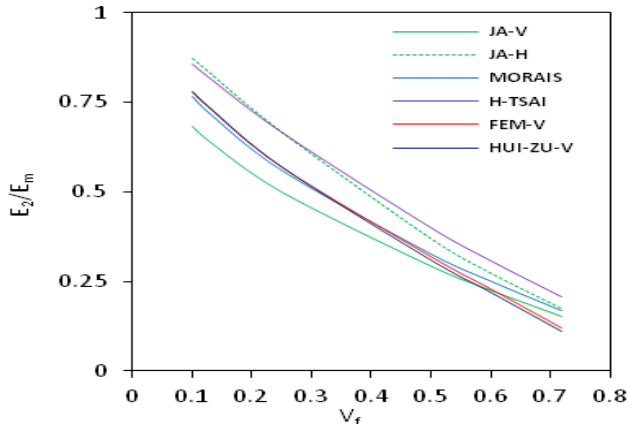

Figure 10. Variation of normalized E_2 with V_f (for E_f /E_m = 5.5:1, fiber like void).

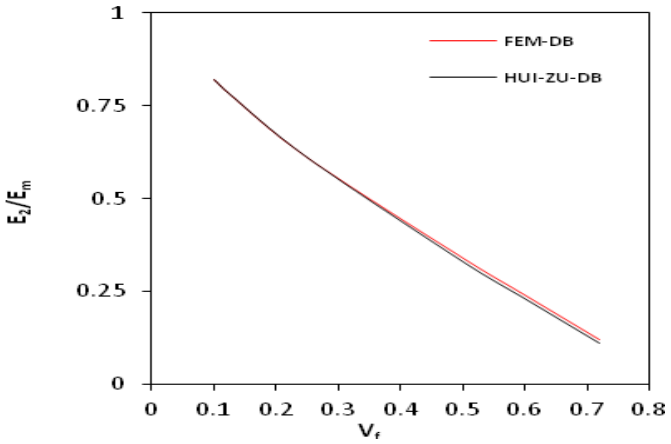

Figure 11. Variation of normalized E_2 with V_f (for E_f /E_m = 5.5:1, total debond).

affected by the variation of E_f/E_m from 100 to 50 in analytical models as much as it has been in FE model. Rather, it could be stated that FE model responds more sensitively to variation of E_f/E_m compared to all analytical models referred here in case of transverse modulus.

The mutual disagreement of analytical models with FE one necessitates verification of the genuinity with an exact analytical model or experimental result. Hui-Zu and Tsu-Wei (1995) have evolved an exact elasticity model for two composites and deteermined E_2 for a range of volume fractions from 10 to 70%. The composite combinations are glass/epoxy with E_f/E_m = 73.1/3.45 (21.19:1) and alumina/aluminum with E_f /E_m = 379/68.9 (5.5:1). Accordingly, E_2 has been determined, for the same combinations of E_f/E_m used by Hui-Zu, with FE and other analytical models. Figures 8 and 9 show the comparison of all the available models in these two cases. Interstingly, for all values of V_f, Hui-Zu and FE models are in very close agreement for both the composites, whereas other analytical models are not so in general and at higher volume fractions in particular. It can be inferred that FE model is a reliable model for a perfectly bonded case.

Further investigation into the cases of fiber like void and fiber-matrix debond is done and the results are compared. Figures 10 and 11 show similar comparisons made for fiber like void and fiber-matrix debond cases, respectively. Those analytical models which ever can yield results in case of fiber like void are compared in Figure 10. Since the other analytical models excepting Hui-Zu's have no provision for total debond, they do not appear in Figure 11. IROM and MIROM have no provision to deal with these two cases and hence do not appear for comparison in both these cases. It is observed that, even in cases of fiber like void and fiber-matrix debond, there is very close agreement between FE and Hui-Zu models that further confirms FEM's reliability.

Comparison of analytical and FE models in matrix dominated cases

Very close agreement between FE and Hui-Zu results in

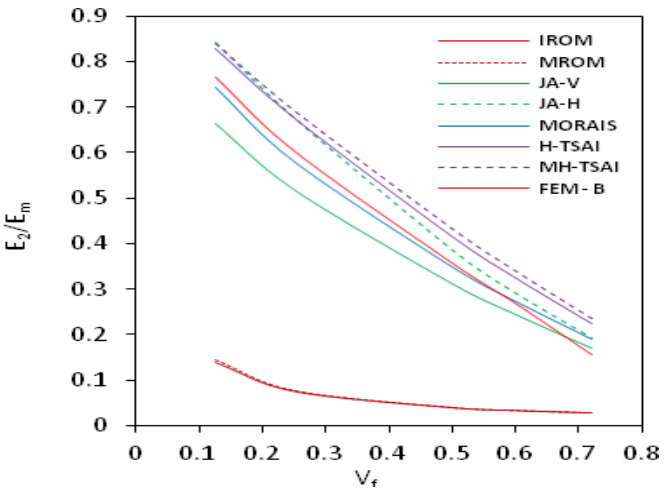

Figure 12. Variation of normalized E_2 with V_f (for E_f/E_m = 1: 50).

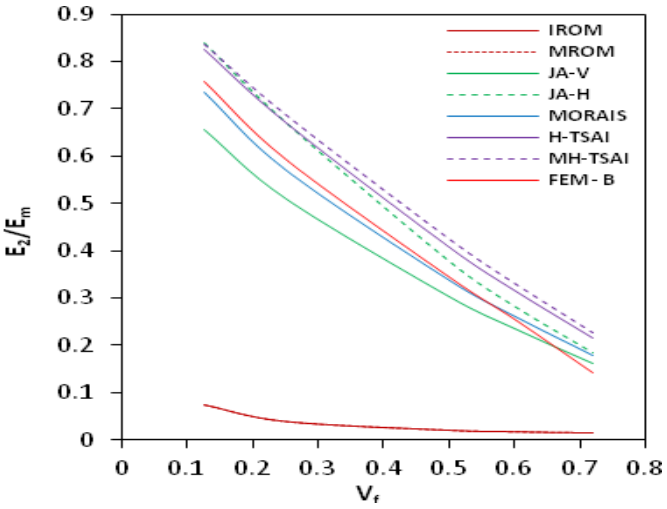

Figure 13. Variation of normalized E_2 with V_f (for E_f/E_m = 1: 100).

all cases viz., perfectly bonded, fiber like void and total debond, confirms the consistency and dependability of these two models. This outcome leads the discussion towards the necessity of comparing FE model with experimental results for further confirmation of its validity. Analytical models' disagreement with FE and Hui-Zu models in cases of $E_f/E_m>1$ prompted the authors to study their behavior in matrix dominated cases ($E_f/E_m<1$) as a matter of academic interest. Figures 12 and 13 show the variation of normalized E_2 with V_f for cases where $E_f/E_m<1$. It can be observed that in matrix dominated cases also IROM and MIROM fail to predict values anywhere near other analytical models' which is their built-in deficiency. Other analytical models are predicting values either above or below but not close to FE model that further raises the ambiguity regarding their consistency.

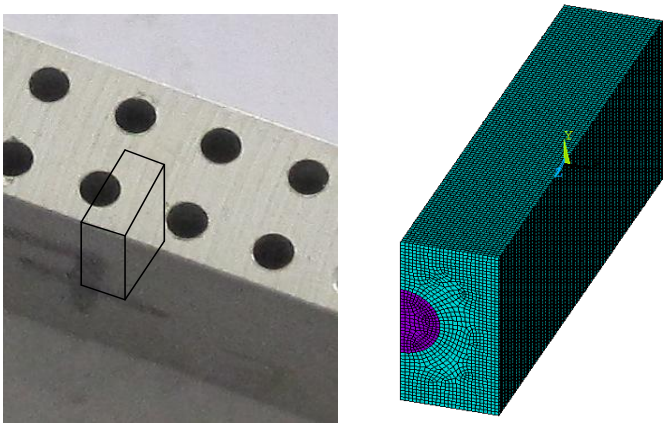

(a) (b)

Figure 14. Modified RVE (a) Highlighted on the specimen; (b) Modified FE model.

Verification of FE with experimental results in case of fiber-matrix de-bond

Though square RVE is acceptable for the present FE analyses, further discussions have led to a situation that prompted the authors to go for suitable modifications of RVE. Thus, FE model of a regular square RVE is modified to suit the specimen conditions such as finite dimensions across the thickness and width and for possible fiber-matrix interface debond. Figures 14(a) and (b) show the modified FE model used for final analysis. Table 3 shows the transverse moduli of the subject composites (V_f = 0.12566) determined from experimental and FE studies. Since the fibers are only inserted into the matrix and not glued, the composites in the present experiment fall into the category of debonded fiber-matrix. Hence, the experimental results are compared with debond case of FE results. The error in case of fiber like void is within the acceptable limits. However, the errors in the cases of other two composites (MS/AL and CU/AL) are slightly higher but not too objectionable. This could be attributed to the type of fit effected between the fiber and matrix surfaces during assembly of fibers in matrix.

Relative closeness of experimental and FE results confirms the dependability of FEM in predicting transverse modulus of fiber reinforced composites. Also this study enables the authors to state that FEM can be extended in micromechanical analysis of composites to study those cases where conventional analytical models are unable to address. Summing up, it can be said that the study not only verifies FEM with experimental results for validation and vice versa as well.

Conclusions

A test specimen that can be exactly modeled in analytical

Table 3. Experimental and FEA results of transverse modulus (GPa) of the subject composites.

Composite material	Experimental results (average)	FEA modified debond case	% error
Mild steel-Aluminum	51.487	49.270	4.30
Copper-Aluminum	51.135	49.217	3.75
Fiber like void-Aluminum	49.412	48.437	2.01

form is designed, fabricated and tested for transverse Young's modulus for three different material combinations viz., mild steel-aluminum, copper-aluminum and fiber like void-aluminum. Identical conditions are simulated using application 3-D FEM in ANSYS soft ware. FE results are found to be in close agreement with exact analytical results available in the literature and also in good agreement with experimental results. Hence, the aim of exploring the capability of FEM for micromechanical analysis of fiber reinforced composites is accomplished.

ACKNOWLEDGEMENTS

The authors gratefully acknowledge the fullest cooperation extended by the management of M/s United Seamless Tubular Pvt. Ltd., and M/s Oil Country Tubular Pvt. Ltd., Narketpally, A.P., India, by according permission to conduct experiments in their laboratory. The authors also express their gratitude to the Principal, V.R. Siddhartha Engineering College, Vijayawada, A.P., India, for permitting them to use their material laboratory.

REFERENCES

Alfredo BM (2000). Transverse moduli of continuous fiber reinforced polymers, Compos. Sci. Technol. 60:997-1002.

Autar KK (1997). Mechanics of Composite Materials, CRC Press.

Bhaskar P, Mohammed RH (2012). Analytical Estimation of elastic properties of polypropylene fiber matrix composite by finite element analysis, Scientific Research. Adv. Mater. Phys. Chem. 2:23-30.

Haktan KZ, Dilek K (2007). A numerical study on the coefficients of thermal expansion of fiber reinforced composite materials. Sci. Direct Compos. Struct. 78:1-10.

Halpin-Tsai JC, Kardos JL (1976). The Halpin-Tsai equations: A review. Polymer Eng. Sci. 16(5).

Hirsch TJ (1962). Modulus of elasticity of concrete affected by elastic moduli of cement paste matrix and aggregate. J. Am. Con. Inst. 59:427.

Hui-Zu S, Tsu-Wei C (1995). Transverse elastic moduli of unidirectional fiber composite with fiber/matrix interfacial debonding. Compos. Sci. Technol. 53:383-391.

Isaac MD, Ori I (1994). Engineering Mechanics of Composite Materials. Oxford University Press.

Jacquet E, Trivaudey F, Varchon D (2000). Calculation of the transverse modulus of a unidirectional composite material and of the modulus of an aggregate: Application of rule of mixtures. Compos. Sci. Technol. 60:345-350.

Kalaprasad G, Joseph K, Thomas S, Pavithran C (1997). Theoretical modeling of tensile properties of short sisal fiber-reinforced low-density polyethylene composites. J. Mater. Sci. 32:4261-4267.

Li DS, Wisnom MR (1994). Finite element micromechanical modeling of unidirectional fiber reinforced metal-matrix composites. Compos. Sci. Technol. 51(4):545-563.

Mistou S, Karama M, Morgado E, Diez J, Schwarz R, Macarico A, Koynov S (2000). Comparative study on the determination of elastic properties of composite materials by tensile tests and ultra sound measurement. J. Compos. Mater. 34(20):1696-1709.

Muhannad ZK, Mustafa SA, Hyder MA (2011). Mechanical properties comparison of four models, failure theories study and estimation of thermal expansion coefficients for artificial E-glass polyester composite. Eng. Tech. J. 29(2):278-292.

Neilson LE (1970). Generalized Equation for the Elastic Moduli of Composite Materials. J. Appl. Phys. 4:4626.

Robert MJ (1999). Mechanics of Composite Materisls, Taylor and Francis.

Stagni L (2001). Effective transverse elastic moduli of a composite reinforced with multilayered hallow cored fibers. Compos. Sci. Technol. 61:1729-1734.

ASTM International (2008). Standard test method for tensile properties of polymer matrix composites materials, D3039/D3039M-08.

Theocaris PS, Stavroulakis GE, Panagiotopoulos PD (1997). Calculation of effective transverse elastic moduli of fiber-reinforced composites by numerical homogenization. Compos. Sci. Technol. 57(5):573-586.

UPCOMING CONFERENCES

International Conference on Mathematical Modeling in Physical Sciences Prague, Czech Republic, September 1-5, 2013

14th International Conference on Accelerator and Large Experimental Physics Control Systems. The Hyatt Regency Embarcadero Center San Francisco, California October 6-11, 2013

Conferences and Advert

September 2013
International Conference on Mathematical Modeling in Physical Sciences
Prague, Czech Republic, September 1-5, 2013

October 2013
14th International Conference on Accelerator and Large Experimental Physics Control Systems. The Hyatt Regency Embarcadero Center San Francisco, California October 6-11, 2013

International Journal of Physical Sciences

Related Journals Published by Academic Journals

- *African Journal of Pure and Applied Chemistry*
- *Journal of Internet and Information Systems*
- *Journal of Geology and Mining Research*
- *Journal of Oceanography and Marine Science*
- *Journal of Environmental Chemistry and Ecotoxicology*
- *Journal of Petroleum Technology and Alternative Fuels*

academicJournals